https://doi.org/10.15407/ujpe68.8.549

M.V. STRIKHA,[1,2] A.M. GORIACHKO[1]

[1] Taras Shevchenko National University of Kyiv,
Faculty of Radiophysics, Electronics, and Computer Systems
(4g, Akademika Glushkova Ave., Kyiv 03022, Ukraine)
[2] V.E. Lashkaryov Institute of Semiconductor Physics, Nat. Acad. of Sci. of Ukraine
(41, Nauky Ave., Kyiv 03028, Ukraine; e-mail: maksym_ strikha@hotmail.com)

SURFACES WITH LOWERED ELECTRON WORK FUNCTION: PROBLEMS OF THEIR CREATION AND THEORETICAL DESCRIPTION. A REVIEW

Experimental studies devoted to the creation of the modern photocathodes or efficient field emission cathodes with lowered work function or low/negative electron affinity are reviewed. We present theoretical models, where the electron affinity lowering is associated with the influence of electrically charged layers at the semiconductor/insulator interface. Modern experimental techniques of measuring the work function or the electron affinity and technologies aimed at fabricating the surfaces with low work function/electron affinity are described.

In the framework of a simple theoretical model developed by the authors, it has been demonstrated that the presence of a dipole layer (e.g., composed of negatively charged oxygen ions and positively charged rare earth ions) at the semiconductor surface can lower the electron affinity by up to 3 eV provided equal concentrations of oppositely charged adsorbate ions. It is also shown that if the surface concentration of negatively charged oxygen ions is higher than the surface concentration of positively charged metal ions, the lowering of the electron affinity becomes smaller due to the upward band bending in the space charge region in the semiconductor; otherwise, the lowering of the electron affinity becomes larger due to the downward band bending. This effect allows technological proposals to be formulated for obtaining surfaces with minimum work function values in modern field-emission-based electronic devices.

In the framework of the proposed model, the work function was evaluated for the OH-functionalized MXene. The corresponding value for the unfunctionalized MXene equals about 4.5 eV, being practically independent of the number of Ti and C layers (from 1 to 9 layers). The OH-functionalization lowers it down to about 1.6 eV, and this value is also practically independent of the number of atomic layers in MXene.

Experimental approaches to obtain cathodes with low work function/low electron affinity are described. They are aimed at creating a spatial separation of electric charges in the near-surface cathode region perpendicularly to the surface plane. The corresponding spatial distributions of positive and negative charges are characterized by their localization either in two different atomic planes or in one plane and an extended space region (the latter variant is typical of semiconductor substrates). The technologies for producing such surfaces are based on various methods of adsorbate deposition onto the metal or semiconductor substrate: physical vapor deposition, chemical vapor deposition, liquid phase deposition, diffusion from the substrate bulk, and so forth. Particular attention is paid to the experimental works dealing with the adsorbtion of rare earth metals (Ce, Gd, Eu) and the coadsorbtion of oxygen onto the Si, Ge, and Mo surfaces (in a nano-structured state as well), which results in the dipole layer formation and the work function reduction.

K e y w o r d s: surface, work function, electron affinity, cathode, dipole layer.

1. Introduction

Negative values of the electron affinity in GaAs crystals, whose surface is covered with a Cs monolayer, were first discovered in 1965 (see work [1] and references therein). At the same time, the electron field emission, for which the lowest possible value of the cathode work function is desirable, still remains the subject of intense research because of numerous applications, such as the creation of flat display panels, electron microscopes, vacuum microelectronics, X-ray sources, powerful microwave sources and amplifiers, and high-current cathodes. This occurs, because the field emission provides high efficiency and brightness in combination with miniature device dimensions (see, for example, works [2,3] and references therein). A reduction of the cathode work function (ideally, a transition to the negative affinity for dielectric and semiconductor cathodes) could substantially improve the parameters of such devices.

Currently, cesium remains to be a widely used material with a low work function of 2.1 eV [4], but its application is severely restricted because of its high toxicity. Long ago, reliable negative electron affinity values were obtained for various diamond surfaces formed by appropriate treatments. A record value of -2.01 eV was obtained for the diamond (100) surface covered with a mixture of magnesium and oxygen atoms [5,6]. However, the efficiency of using diamond as a cathode is limited, because it is an insulator, so only a low crystal doping level with the use of the ionic implantation can be provided [7]. Therefore, the rate of supplying carriers from the crystal bulk to the emission surface is low.

Therefore, under consideration are alternative ways of creating the cathodes on the basis of the adsorption of alkaline and rare earth (Ce, Gd, Eu) metals and the coadsorption of oxygen on the Si, Ge, and Mo surfaces (in a nanostructured state as well), where charge double layers can be formed, which substantially reduces the work function [8,9]. In recent years, special attention has been attracted by a new class of materials, Mxenes; using the OH-termination of their surface, the corresponding work function can be diminished to values of about 1 eV [10].

The theoretical description of the work function reduction under the influence of adsorbed layers was first carried out in the framework of either a simple dipole model (see, e.g., work [11]), which did not consider the possibility of the formation of a space charge region (SCR) in the semiconductor, or complicated (and with no demonstrativeness) calculations from first principles (see, e.g., works [12, 13]). Recently, a rather illustrative theoretical model has been developed [14,15], which involves the influence of both the charge of adsorbed layers and the charge of the SCR emerging under the semiconductor surface. The application of this model to Mxenes [16] demonstrated a good agreement with the results of calculations from first principles.

2. Electron Work Function of Solid Surface. Basic Physics. Kohn–Sham Equation

The work function is one of the fundamental characteristics of the electronic subsystem of solids. It is defined as the energy distance between the Fermi and vacuum levels [17–19]. In metals at the temperature $T = 0$ K, the work function is equal to the minimum energy required to move an electron from a solid to an infinitely large distance from it. The metal work function is just a parameter that best characterizes the efficiency of the material application for fabricating the cold cathodes (field emitters) and cathodes of other types.

In semiconductors and insulators, except for the cases of their high doping to the degenerate state, the Fermi level is located in the forbidden gap, so it has no electrons, and there is no emission from it into the vacuum. Therefore, a more relevant semiconductor parameter from the viewpoint of the material efficiency for cathode applications is the electron affinity, i.e., the energy of the conduction band bottom reckoned from the vacuum level. Electrons can appear in the conduction band of a semiconductor at non-zero temperatures due to their thermal activation from the impurity levels or the valence band. In addition, they can be introduced by external streams in spatially heterogeneous and non-equilibrium structures.

In all those cases, electrons can turn out, in principle, at any energy level in the conduction band. The-

Citation: Strikha M.V., Goriachko A.M. Surfaces with lowered electron work function: Problems of their creation and theoretical description. A review. *Ukr. J. Phys.* **68**, No. 8, 549 (2023). https://doi.org/10.15407/ujpe68.8.549.

Цитування: Стріха М.В., Горячко А.М. Поверхні зі зниженою роботою виходу: проблеми створення та теоретичного опису. Огляд. *Укр. фіз. журн.* **68**, №8, 551 (2023).

refore, strictly speaking, it is not possible to determine the minimum energy required to remove one electron from a solid. At the same time, it is most likely that, as a result of relaxation processes, the electron will turn out at the level with the lowest energy in the conduction band, i.e., at the conduction band bottom. That is why the electron affinity is just the most characteristic height of the potential barrier that the electron overcomes when escaping from the semiconductor into the vacuum, which is a crucial factor when estimating the efficiency of the semiconductor cathode.

The electronic subsystem of a solid is essentially a multiparticle system. Therefore, in the most general case, the energy that must be spent to remove an electron from a solid is determined by the expression:

$$\Delta E = E(N) - E(N-1), \tag{1}$$

where $E(N)$ is the total energy of the multiparticle system containing N particles (before the electron emission into vacuum), and $E(N-1)$ is the energy of the system of $N-1$ particles (after the electron emission). The exact calculation of the total energy of a multielectron system without any approximations is known to be impossible for any practically relevant number of electrons: neither analytically, nor numerically. In this connection, the one-electron approximation is used, as a rule, and the total energy of the system is calculated in the framework of the density functional theory [20]. For the development of this theory, the American scientist Walter Kohn (1923–2016) won the 1998 Nobel Prize in chemistry.

The basic equation of the density functional theory is the Kohn–Sham equation [21]. For spin-unpolarized systems, it looks like

$$\left[-\frac{\nabla^2}{2}+V_n(\mathbf{r})+V_{\rm H}(\mathbf{r})+V_x(\mathbf{r})+V_c(\mathbf{r})\right]\phi_i(\mathbf{r}) = \varepsilon_i\phi_i(\mathbf{r}). \tag{2}$$

In essence, this equation is a one-particle stationary Schrödinger equation for a certain fictitious system of particles. The potential energy operator in the Hamiltonian of this equation consists of the following components: $V_n(\mathbf{r})$ is the potential of electron interaction with point-like electric charges of atomic nuclei (they are considered to be fixed in space), $V_{\rm H}(\mathbf{r})$ is the Hartree potential of electron interaction with the spatially distributed electric charges of all other electrons in the system, $V_x(\mathbf{r})$ is the exchange interaction potential in the electron subsystem, and $V_c(\mathbf{r})$ is the correlation energy potential in the electron subsystem; ε_i are the Kohn–Sham eigen energies, and $\phi_i(\mathbf{r})$ are the Kohn–Sham wave functions. The subscript i enumerates the states, which can be occupied or not; the number of occupied states must be equal to the number of electrons in the system, N.

In the general case, the variation of N changes the spatial distribution of the total electron density

$$n(\mathbf{r}) = \sum |\phi_i(\mathbf{r})|^2, \tag{3}$$

where the summation over i is carried out from 1 to N in the ε_i-ascending order. The operators $V_{\rm H}(\mathbf{r})$, $V_x(\mathbf{r})$, and $V_c(\mathbf{r})$ – and, therefore, all ε_i and $\phi_i(\mathbf{r})$ – functionally depend on $n(\mathbf{r})$. This means that the Kohn–Sham equations (2) written for a multielectron system are interconnected, and the system of such equations can be solved only using iterative methods. It is important to understand that, in the general case, ε_i and $\phi_i(\mathbf{r})$ cannot be considered as the energies and wave functions of individual electrons. They are only mathematical constructions created for determining the electron density $n(\mathbf{r})$ in the ground state.

It is worth noting that, owing to the translational symmetry of crystalline solids, the wave functions in the Kohn–Sham equations (2) are Bloch-like, i.e., they can be written in the form $\phi_{i\mathbf{k}}(\mathbf{r}) = e^{i\mathbf{kr}}u_{i\mathbf{k}}(\mathbf{r})$, where $u_{i\mathbf{k}}(\mathbf{r})$ is a coordinate-dependent function with the spatial periodicity of the crystal lattice. In this notation, the subscript i begins to play the role of the energy band index, and $\mathbf{k}$ is a wave vector that actually enumerates the Kohn–Sham energy $\varepsilon_{i\mathbf{k}}$. The functions $u_{i\mathbf{k}}(\mathbf{r})$ satisfy the special Kohn–Sham equations

$$\left[-\frac{1}{2}\left(\nabla + i\mathbf{k}\right)^2 + V_{\rm tot}(\mathbf{r})\right] u_{i\mathbf{k}}(\mathbf{r}) = \varepsilon_{i\mathbf{k}}u_{i\mathbf{k}}(\mathbf{r}), \tag{4}$$

where the potential energy operator is the same as in the standard Kohn–Sham equations:

$$V_{\rm tot}(\mathbf{r}) = V_n(\mathbf{r}) + V_{\rm H}(\mathbf{r}) + V_x(\mathbf{r}) + V_c(\mathbf{r}).$$

To determine the action of the operators $V_{\rm H}(\mathbf{r})$, $V_x(\mathbf{r})$, and $V_c(\mathbf{r})$, we have to know the electron density (3). In this version of Kohn–Sham equations, it is calculated as follows:

$$n(\mathbf{r}) = \sum_i \int\limits_{\rm BZ} \frac{d\mathbf{k}}{\Omega_{\rm BZ}} f_{i\mathbf{k}} \left|u_{i\mathbf{k}}(\mathbf{r})\right|^2, \tag{5}$$

where the summation is performed over all found solutions of the Kohn–Sham equations, the integral is taken over the Brillouin zone in the reciprocal crystal lattice, and $f_{i\mathbf{k}} = 1$ for occupied and 0 for unoccupied ststes; the occupation of states is assumed to take place in the $\varepsilon_{i\mathbf{k}}$-ascending order until the equality between the integral of this electron density over the unit cell volume and the number of electrons per unit cell is reached.

An important simplification consists in that the variation of the electron density in a macroscopic solid owing to the addition or subtraction of a single electron can be completely neglected. In this approximation, $\varepsilon_{i\mathbf{k}}$ is equal to the system energy decrease, if an electron is removed from the state with the subscripts $i\mathbf{k}$, or to the system energy growth, if the electron occupies this state [22]. This is a very important approximation, because it allows the eigenenergies of the Kohn–Sham equations (4) to be used to determine the work function or the electron affinity. For this purpose, they should be correlated with the vacuum level, which is, by definition, the energy of an electron at rest at a sufficiently large distance from the solid.

This procedure is performed by iteratively solving the Kohn–Sham crystal equations for a sufficiently large space volume, which includes the solid itself, its surface, and the vacuum. In effect, the calculations are carried out for a certain artificial atomic construction, the so-called "slab", which is periodic along all three orthogonal coordinate axes. The spatial period along the direction perpendicular to the surface plane includes a certain number of unit cells (atomic layers) of the crystalline structure of the examined substance and a certain gap – vacuum gap – free of any atoms.

The vacuum level is taken as the potential energy of the electron in the potential $V_n(\mathbf{r}) + V_{\mathrm{H}}(\mathbf{r})$ inside the vacuum gap, i.e., at the maximum possible distance from the simulated surface and the layers composing the neighbor slab. It is intuitively clear that if the vacuum gap is sufficiently thick, the electron density near its central part is practically zero, so the exchange and correlation energies are also equal to zero, and it is enough to consider only the electrostatic potential energy, which is a trivial task, because the operators $V_n(\mathbf{r})$ and $V_{\mathrm{H}}(\mathbf{r})$ are simple scalars. After finding the vacuum level, the energy difference between it and the highest $\varepsilon_{i\mathbf{k}}$-value corresponding to $f_{i\mathbf{k}} = 1$ is equal to the work function for the metal. In the case of a semiconductor, the energy difference between the vacuum level and the lowest $\varepsilon_{i\mathbf{k}}$-value corresponding to $f_{i\mathbf{k}} = 0$ gives the value of the electron affinity.

The procedure of numerical calculations of the work function and the electron affinity described above is characterized by considerable difficulties in its practical application. First of all, the electronic structure of the solid (in particular, the quantities $\varepsilon_{i\mathbf{k}}$ and $n(\mathbf{r})$ near the solid surface, which terminates the semiinfinite crystalline structure of the solid) has to be reproduced as best as possible. This circumstance dictates the simulation of slabs with as many atomic layers of the substance as possible. In addition, for a more accurate reproduction of the vacuum level, it is necessary to choose a slab whose vacuum gap is as wide as possible. Furthermore, due to the surface reconstruction or the formation of ordered structures from foreign adsorbed atoms, the spatial periods of the slab along the solid surface can rather often be several times larger than the corresponding spatial periods of a unit cell in the crystalline structure of the corresponding metal or semiconductor.

All those factors result in that the translationally symmetric volume of the slab, where the Kohn–Sham system of equations has to be solved, can be two or, in extreme cases, three orders of magnitude larger than the volume of a unit cell in the depth of the crystalline structure of the corresponding substance, which extremely strongly increases, demands the necessary computing resources. It is also worth noting that even if those resources are available, such a calculation is far from routine; it rather resembles a full-blown process of unique scientific research. This occurs due to the necessity of choosing the exchange-correlation energy functionals. There are plenty of them, and each of them is specifically designed for the optimal reproduction of certain physical properties in certain classes of substances and materials.

In order to reduce the amount of calculations, the system of Kohn–Sham equations is not solved for all electrons in the solid, but only for electrons in unfilled atomic shells. Therefore, there also arises the necessity to choose the pseudopotentials describing the electric field of ionized cores.

Additional calculations may also become necessary, if the crystalline structure of the near-surface layers in the solid and/or the adsorbed layers of foreign atoms is a priori unknown. In this case, the equilibrium positions of atomic nuclei have to be searched for by

minimizing the Gell-Mann–Feynman forces [22] in the researched system. A modern example of such calculations for tungsten surfaces with an adsorbed layer of barium and oxygen (as a basis of ordinary thermionic cathodes) can be found in work [23] and, for two-dimensional materials, in work [24]. Databases of calculated work functions for various elements and crystallographic surface orientations are also created [25].

The procedures described above can be simplified for metals using the jellium model for the homogeneous electron gas (the term jellium is formed as a combination of the root jelly and the ending typical of the metals' names; for details, see work [26] and references therein). In this model, instead of positively charged ionic cores, the isotropic and continuous positive charge equal by magnitude to the total charge of ions is considered. This model rather well describes simple metals such as Na, Mg, and Al, where the conduction band is formed by the s- and p-electronic orbitals.

The jellium model is especially convenient when considering surface problems, in particular, when determining the work function. For a semiinfinite specimen with the z-axis directed perpendicularly to the surface, the distribution of the uniform positive charge $n^+(z)$ in the jellium model looks like a step:

$$n^+(z) = \begin{Bmatrix} \bar{n}, z \le 0 \\ 0, z > 0 \end{Bmatrix}. \tag{6}$$

Now, the electron density (3) must have the following boundary conditions:

$$n(z) = \begin{Bmatrix} \bar{n}, z \to -\infty \\ 0, z \to +\infty \end{Bmatrix}. \tag{7}$$

The quantity $\bar{n}$ in Eq. (6) can be easily determined, e.g., from Hall measurements, or evaluated from the parameters of the metal crystal lattice, assuming that every ion produces one conduction electron.

For the first time, the calculation of the electron density profile in the ground state in the jellium model using the density functional method and the homogeneous electron gas approximation (the so-called local density approximation) was carried out in work [27]. It was shown that the electron density extends beyond the crystal boundary by 1–3Å. As a result, there emerges a disbalance between the positive and negative charges in the near-surface region, and there appears a dipole layer whose minus is located outside the crystal, and plus inside it. It was also shown that the electron density (7) approaches the value $\bar{n}$ in the crystal depth by oscillating with the period π/k_{F}, where

$$k_{\mathrm{F}} = (3\pi\bar{n})^{1/3} \tag{8}$$

is the Fermi vector. Such Friedel oscillations are the electron gas response to the break in the positive charge distribution at the crystal surface [Eq. (6)].

Having found, in the framework of the jellium model, the dependence $V_{\mathrm{tot}}(z)$ of the total potential energy V_{tot} entering Eq. (4) on the coordinate z, we can write the obvious expression for the work function:

$$W = V_{\mathrm{tot}}(+\infty) - V_{\mathrm{tot}}(-\infty) - E_{\mathrm{F}}. \tag{9}$$

Here, the Fermi energy is approximately equal to

$$E_{\mathrm{F}} = \frac{\hbar^2 k_{\mathrm{F}}^2}{2m} = \frac{\hbar^2}{2m}(3\pi\bar{n})^{2/3}. \tag{10}$$

Following this scheme, the work function values were already obtained in work [4] for some metals (Al, Zn, Pb, Mg, Li, Na, K, Rb, Cs), and the calculation data corresponded well enough to experimental data. However, the implementation of even such a simplified scheme also requires cumbersome numerical calculations. Moreover, the jellium model was developed for metals and describes significantly worse semiconductors and insulators with low electron gas densities.

Without denying the necessity of carrying out the first-principle calculations as the most modern and most complete theoretical approach to finding the values of the work function for metals and the electron affinity for semiconductors, it is also possible to talk about the obvious need to create simple and clear empirical models that provide sufficiently accurate and, at the same time, simple analytic estimates of those quantities [28, 29].

3. Theoretical Model to Describe the Reduction of Work Function under the Influence of Surface Charge Layers

The physical origin of negative electron affinity values is easy to understand: it is a result of the presence of a double charge layer near the semiconductor surface, where the positive charge is located outside, and thus

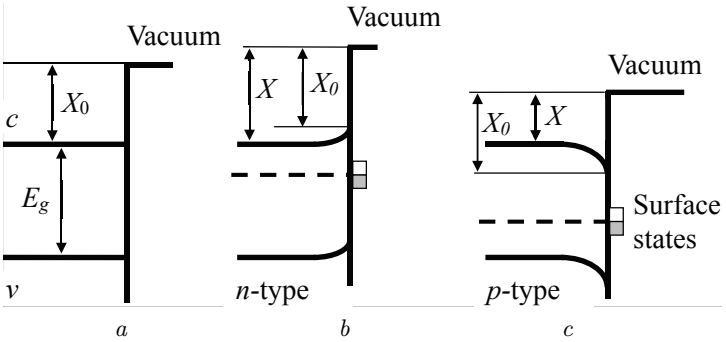

Fig. 1. Influence of surface states on the electron affinity value X with respect to vacuum: an idealized case without surface states, $X = X_o$ (a); in n-type materials, $X > X_o$ (b); in p-type materials, $X < X_o$ (c). The dashed line designates the Fermi level

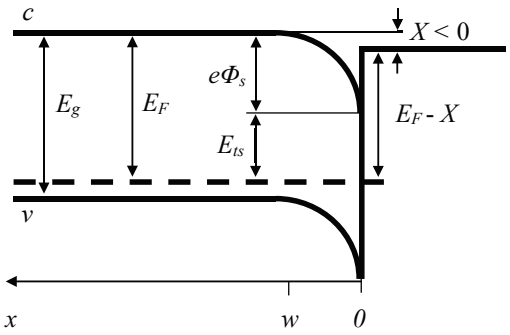

Fig. 2. Emergence of negative electron affinity, $X < 0$ [14]. The dashed line designates the Fermi level

reduces the electron potential in the vacuum. However, the mechanism of formation of such a layer can be different [14].

Let us first consider a semiconductor or an insulator with the band gap E_g and the electron affinity X_o. An idealized case without surface levels is shown in Fig. 1, a. However, if such levels are available (and they do exist at all real solid-vacuum interfaces [30, 31]), a space charge region is formed near the surface, which gives rise to the band bending. In the n-type semiconductor, the establishment of an equilibrium between the bulk and surface states gives rise to an upward band bending (the barrier prevents the capture of new electrons from the bulk onto those states). Therefore, the electron affinity to vacuum X in those materials exceeds X_o (Fig. 1, b).

On the contrary, in the case of p-type material, the capture of holes from the bulk and the formation of a localized positive charge at the surface stimulates the appearance of the downward band bending (similarly, the barrier prevents the capture of new holes from the bulk onto impurity states). This, however, decreases the affinity value, $X < X_o$ (Fig. 1, c). The physical origin for this decrease is a charge double layer: positive charges localized immediately at the surface and negative charges (both localized and mobile) beneath.

If the downward band bending is large enough, a situation with the negative affinity may arise (Fig. 2). Indeed, the near-surface band bending $e\Phi_s$ is related to the energy E_{ts} of surface states and the Fermi level $E_{\rm F}$ in a semiconductor (the energies are reckoned from the bottom of the conduction band, and the energy axis in Fig. 2 is directed downward) via the obvious relation

$$e\Phi_s = E_{\rm F} - E_{ts}. \tag{11}$$

On the other hand, for the electron affinity X, the following expression is valid:

$$X = X_o - e\Phi_s. \tag{12}$$

One can see from Eq. (12) that if the near-surface band bending $e\Phi_s$ exceeds X_o, the electron affinity becomes negative (Fig. 2).

The above consideration concerns an idealized case of surface states, each with a single energy level E_{ts}. Usually, the surface states are more or less "smeared" against the background of the energy spectrum in the semiconductor band gap and are described by a certain energy density of states $D(E)$. Under such conditions, the quantity E_{ts} in Eq. (11) is a solution of the integral equation resulting from the requirement

that the surface states be half-filled [14],

$$\int_0^{E_{ts}} D(E)dE = \frac{1}{2}\int_0^{\infty} D(E)dE. \tag{13}$$

Equation (13) (it is written for singly charged centers) can be solved only in the framework of certain model approximations. Therefore, without loss of generality, we consider below the one-level case, $D(E) = \delta(E - E_{ts})$.

Using the Poisson equation, the band bending (11) can be related to the concentration ρ of a bulk charge in the semiconductor (measured in C/m^3-units) and the surface charge density eN_s,(measured in C/m^2-units),

$$\frac{d^2\Phi(x)}{dx^2} = -\frac{\rho}{\varepsilon_o\varepsilon_s}, \tag{14}$$

where ε_o is the dielectric constant of vacuum, and ε_s the dielectric constant of the semiconductor. Equation (14) can be supplemented with obvious boundary conditions: the zero values of the potential and its first derivative at the boundary w of the space charge region,

$$\Phi(w) = 0, \quad \left.\frac{d\Phi(x)}{dx}\right|_{x=w} = 0. \tag{15}$$

Equation (14) with boundary conditions (15) can be solved analytically in the depletion approximation, i.e., when the band bending is such that the majority charge carriers (holes) are already absent from the space charge region, whereas electrons are still absent, so the charge is determined here exclusively by the difference between the localized charges of the ionized acceptors and donors:

$$\rho(x) = \begin{cases} e(N_a - N_d), & \text{if } 0 < x < w, \\ 0, & \text{if } x \geq w. \end{cases} \tag{16}$$

After substituting Eq. (16) into Eq. (14), the resulting equation is easily integrated. Taking Eq. (15) into account, we get the known result for $\Phi_s \equiv \Phi(0)$:

$$\Phi_s = \frac{e(N_a - N_d)w^2}{2\varepsilon_o\varepsilon_s}. \tag{17}$$

The width of the space charge region is determined from the equality condition between the bulk charge and the charge of the surface states,

$$e(N_a - N_d)w = eN_s. \tag{18}$$

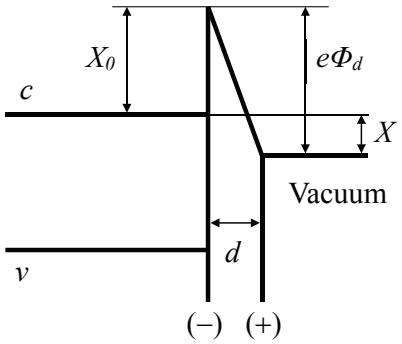

Fig. 3. Reduction of electron affinity by a charge double layer formed by two planes of differently charged adsorbed atoms (adapted from [14])

Substituting Eq. (18) into Eq. (17), we finally obtain

$$\Phi_s = \frac{eN_s^2}{2(N_a - N_d)\varepsilon_o\varepsilon_s}. \tag{19}$$

According to this formula in view of the Weitz limit (only one of 100 or 1000 atoms in the surface monolayer can be in the charged state [31]), the near-surface band bending in a semiconductor with a standard dielectric permittivity of 10 and the moderate doping level $N_a - N_d = 10^{23}$ m^{-3} is about 2 eV [14]. According to Eq. (12), such a value can significantly reduce the affinity value.

Note that the applicability of formula (19) is restricted to the case of relatively small band bendings (to about half the band gap width E_g). Larger band bendings correspond to the conductivity inversion, when a substantial number of free electrons appear in the near-surface region, and the depletion approximation (16) is no longer applicable. However, at the qualitative level, the generality of our conclusions does not change.

Another mechanism giving rise to the formation of a charge double layer was also considered in work [14]. It can be realized in insulators and weakly doped semiconductors (Fig. 3, *b*). Let a layer of negatively charged oxygens be formed immediately on the surface, and let a layer of positively charged alkaline or rare earth metal atoms (e.g., cesium, cerium, and others) cover it. Figure 3 demonstrates an idealized schematic diagram for the case where the surface charge densities in both layers are identical by absolute value and equal to $\pm eN_s$. Surely, this is not true in the general case, and a band bending similar to that considered above is also formed in the

bulk, which compensates the difference between layers' charges. We neglect this phenomenon in the first approximation.

Since the thin gap d between differently charged atomic layers is an order of the interatomic distance, it is transparent for the tunneling of thermal electrons near the conduction band bottom (their wavelength is an order of magnitude larger), which, therefore, can freely tunnel into the vacuum. Hence, the effective electron affinity in this case equals

$$X = X_o - e\Phi_d. \tag{20}$$

The last term on the right-hand side of Eq. (20) can be easily evaluated from the formula for a plane capacitor,

$$\Phi_d = \frac{eN_s d}{\varepsilon_o \varepsilon}, \tag{21}$$

where ε is the dielectric constant of the gap between the charged layers.

Taking $N_s \approx 5 \times 10^{18}$ m^{-2} and putting $\varepsilon \approx 5$ and $d \approx 2 \times 10^{-10}$ m, we obtain $\Phi_d \approx 3$ V. Thus, the indicated mechanism of formation of a charge double layer can also substantially reduce the work function or even can give the negative electron affinity. It is worth to note that such a mechanism can reduce the affinity for any type of bulk conductivity (electron, hole, or intrinsic) rather than only in p-type materials, as the mechanism illustrated in Fig. 2 does.

From Eqs. (11) and (12), it follows that the negative electron affinity is most easily realized in materials with $E_g > X_o$. From this viewpoint, it is clear that diamond (C, $E_g = 5.5$ eV, $X_o = 0.5$ eV) is a good candidate for creating an efficient photocathode. As was shown in many works (see, in particular, work [32]), the (001) and (110) diamond surfaces covered with atomic hydrogen have a negative electron affinity. At the same time, those diamond surfaces, but atomically pure, have an affinity of about 0.6 eV, whereas the same surfaces covered with atomic oxygen have an affinity of about 1.5 eV. The negative affinity decreases the field emission threshold for a diamond cathode approximately three times: from about 80 to 25 V/μm.

From the same viewpoint, we may expect the appearance of effective devices based on silicon carbide β-SiC ($E_g = 2.5$ eV, $X_o = 2$ eV). The creation of promising cathodes on its basis for the field emission has already been reported [33].

At the same time, the negative affinity can be realized not only in insulators and wide-bandgap semiconductors, but also in GaAs covered with a Cs monolayer, which ensures a large localized surface charge and, accordingly, a strong band bending [Eq. (15)] compensating the high value $X_o = 4.5$ eV (see work [1] and references therein). From this viewpoint, also promising is the creation of cathodes based on the adsorption of alkaline and rare earth (Ce, Gd, Eu) metals and the coadsorption of oxygen on the Si, Ge, and Mo surfaces (in the nanostructured state as well), where charge double layers that substantially diminish the work function can also be formed (see Fig. 3).

For instance, it was shown in work [8] that, after some adsorption cycles of Gd atoms and O atoms on the Si(100)-2×1 surface at room temperature and subsequent annealing, the obtained structure at $T \approx 600$ °C had the work function decreases from 4.8 eV to values smaller than 1 eV. In work [9], it was shown that the presence of cerium in submonolayer amounts on the Mo(112) surface reduces the work function of this surface by a value up to 2.2 eV depending on the specific type of adsorbate ordering.

However, the equality $N_s^{(-)} = N_s^{(+)}$ (this case is depicted in Fig. 3) can be provided with high accuracy in real structures only by applying the sophisticated and expensive molecular beam epitaxy technology (if the matter does not concern the adsorption of permanent dipoles on the surface; the case of MXene terminated by hydroxyl OH groups was considered in works [12, 16]). The application of simpler and more affordable technologies for depositing monolayers (CVD and others) inevitably violates the equality $N_s^{(-)} = N_s^{(+)}$. However, a difference of only 0.1% between the concentrations of adsorbates during the monolayer formation brings about the appearance of a surface charge corresponding to the Weitz limit by order of magnitude [31]. As a result, there appears an SCR in the semiconductor and, accordingly, the band bending whose sign is determined by the charge sign of the adsorbate with the higher concentration. Such a band bending considerably affects the electron affinity value, increasing it in some cases and decreasing it in others (see [15, Figs. 4, *c* and 4, *d*]).

In the case $N_s^{(-)} = N_s^{(+)}$ (Fig. 3), since a barrier with interatomic thickness is transparent for the tunneling of electrons located near the conduction band

bottom in the semiconductor, the reduction of the electron affinity is described by formulas (20) and (21), where $N_s \equiv N_s^{(-)} = N_s^{(+)}$ in Eq. (21).

Consider the case where $N_s^{(-)} > N_s^{(+)}$ (Fig. 4, *a*). Then, as was shown in work [15], the left "effective plate" of the capacitor in formula (21) already has a charge equal to the negative charge of the adsorbate plane minus the positive charge of SCR in the semiconductor, which balances the positive charge of the right plate. So,

$$\Phi_d = \frac{eN_s^{(+)}d}{\varepsilon_o\varepsilon}, \tag{22}$$

and the total surface charge of adsorbates with the density $e(N_s^{(-)} - N_s^{(+)})$ corresponds to the charge (with the opposite sign) of the SCR in the semiconductor. Such a charge stimulates the band bending near the surface. In the depletion approximation, the surface potential value can be easily found using a standard procedure of integrating the corresponding Poisson equation. As a result, formula (19) becomes modified:

$$\Phi_s = \frac{e(N_s^{(-)} - N_s^{(+)})^2}{2(N_s d - N_a)\varepsilon_o\varepsilon_s}. \tag{23}$$

Note that formula (23) was obtained for the case of moderate doping, when the Fermi level is located deep enough in the semiconductor band gap, and the depletion approximation remains applicable even for the largest band bendings. Note also that the SCR width in semiconductors with not too high doping levels is equal to about several microns and exceeds the de Broglie wavelength of thermal electrons (nanometers) by orders of magnitude [30]. Therefore, the electron tunneling from the semiconductor bulk through the SCR barrier is impossible, and, as one can see from Fig. 4, *a*,

$$X = X_o + e\Phi_s - e\Phi_d \tag{24}$$

in this case.

So, in the case $N_s^{(-)} > N_s^{(+)}$, the affinity value turns out higher than in the case $N_s^{(-)} = N_s^{(+)}$. From the viewpoint of obtaining the minimum work function, this is an obviously undesirable effect.

In the opposite case, i.e., $N_s^{(-)} < N_s^{(+)}$, the total positive charge of adsorbates is compensated by the formation of a negatively charged SCR in the semiconductor, which is accompanied by a downward band bending (Fig. 4, *b*). Then formula (22) is still valid, whereas formulas (23) and (24) undergo obvious modifications:

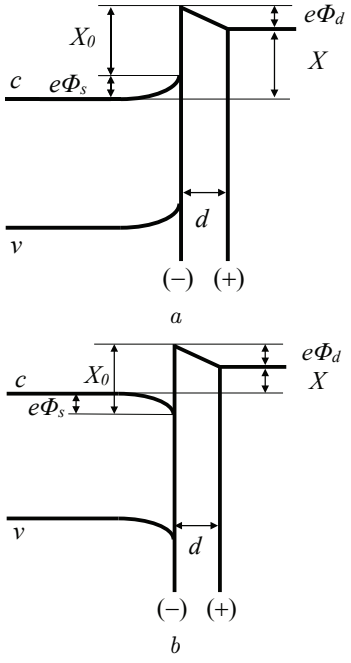

Fig. 4. Appearance of SCR with upward band bending under the condition $N_s^{(-)} > N_s^{(+)}$ (*a*) and downward band bending under the condition $N_s^{(-)} < N_s^{(+)}$ (adapted from [15]) (*b*)

$$\Phi_s = \frac{e(N_s^{(+)} - N_s^{(-)})^2}{2(N_d - N_a)\varepsilon_o\varepsilon_s}, \tag{23a}$$

and

$$X = X_o - e\Phi_s - e\Phi_d. \tag{24a}$$

respectively. As one can see from Eq. (24a), in the case $N_s^{(-)} < N_s^{(+)}$, the affinity value turns out lower than in the case $N_s^{(-)} = N_s^{(+)}$. From the viewpoint of obtaining a surface with the minimum work function for electronic emission devices, this effect is quite desirable. Furthermore, it suggests a technological algorithm for creating such a surface: during the coadsorption of oxygen and metal atoms onto the semiconductor surface, the metal concentration must prevail.

Let us evaluate the magnitude of this effect. Substituting Eqs. (22) and (23a) into Eq. (24a), we obtain

$$X = X_o - \frac{e^2 N_s^{(+)} d}{\varepsilon_o\varepsilon}\left[1 + \frac{\left(N_s^{(+)} - N_s^{(-)}\right)^2 \varepsilon}{2(N_d - N_a)N_s^{(+)} d\varepsilon_s}\right]. \tag{25}$$

For a moderate doping level $N_d - N_a = 10^{22}$ m^{-3}, the surface concentration of metal in the monolayer $N_s^{(+)} \approx 5 \times 10^{18}$ m^{-2}, the oxygen concentration in the monolayer only 0.1% lower than $N_s^{(+)}$, $\varepsilon_s = 10$, $\varepsilon \approx 5$, and $d \approx 2 \times 10^{-10}$ m, we obtain that the magnitude of the second term in the brackets in formula (25) is of order 1. Hence, the affinity reduction induced by the downward band bending in the SCR has the same order of magnitude as the reduction occurring due to the presence of the charge double layer of adsorbates in the case $N_s^{(-)} = N_s^{(+)}$, when the SCR is not formed. However, the depletion approximation used by us is not applicable at such large band bendings (there appears a region of inverse conductivity near the surface), and formula (25) can be used only for the qualitative evaluation of the described effect.

Thus, in works [14, 15], it was shown that the presence of a dipole layer (for example, composed of negatively charged oxygen atoms and positively charged atoms of a rare-earth metal) on the semiconductor surface can decrease the affinity by a valuef o up to 3 eV, if the concentrations of differently charged adsorbed atoms are identical, $N_s^{(-)} = N_s^{(+)}$. An asymmetry between the surface concentrations of oxygen and metal atoms can have two opposite consequences. If negatively charged oxygen atoms prevail, $N_s^{(-)} > N_s^{(+)}$, the affinity reduction is smaller due to the upward band bending in the SCR of the semiconductor. If positively charged metal atoms prevail, $N_s^{(-)} < N_s^{(+)}$, the affinity reduction grows due to the downward band bending. This result allows us to propose technological solutions for obtaining the surfaces with the minimum work function to produce emission electronic devices. The resulting formula (19) can be used to numerically describe the effect at moderate doping, when the Fermi level remains deeply in the band gap, and the depletion approximation remains valid even for the largest band bendings.

4. Work Function Reduction in MXenes with Hydroxyl Termination

In work [16], on the basis of the theoretical model developed in works [14, 15], a substantial reduction of the work function in MXenes $Ti_{n+1}C_n$ with hydroxyl termination was explained and evaluated.

MXenes compose a class of two-dimensional materials. They were described for the first time in 2011 in work [34] co-authored by a native of Ukraine Yuriy Gogotsi, who, despite his long work in the USA, continues to hold a professorship position at Sumy State University. The general MXene formula $M_{n+1}X_nT_x$ includes $n+1$ atomic layers of transition metal M (denoted as M_{n+1}) alternating with n monatomic layers of carbon or nitrogen (X_n); this "sandwich" structure can be terminated from both sides by various terminators (F, O, Cl, OH) denoted as T_x (see Fig. 5). Currently, the term "multilayer MXene" is understood as a structure with five or more layers of a transition metal.

The unique characteristics of MXenes have drawn general attention. According to calculations in work [35], the papers dealing with MXenes were published in more than 400 journals during the decade after their discovery. Those papers were co-authored by more than 8300 researchers from 1450 institutions in 62 countries. Owing to their diverse stoichiometry and surface organization, MXenes possess a wide range of controllable physical and chemical properties. For instance, the width of the band gap in MXenes can vary, which depends on the method of surface termination. MXenes have high electrical conductivity, high elastic modulus, ultra-low optical attenuation, and so forth. Nowadays, MXenes are used in energy storage and conversion devices, electronics, sensors, medicine, and so forth (see review [36] and references therein).

One of the domains of the potential application of MXenes is the creation of cathodes with low work function for emission electronics. In work [12], on the basis of first principles, the work function of MXenes functionalized with surficial O, F, and OH was calculated. It was shown that the functionalization with oxygen or fluorine results in a small decrease or increase of the work function, whereas hydroxyl-terminated MXenes can exhibit low work function in an interval from 1.6 to 2.8 eV. The main relevant factor of the work function reduction is the intrinsic dipole moment of the hydroxyl OH group.

The computations in work [12] were carried out using extensive software packages, and, therefore, lack simple qualitative apparency. That is why a simple theoretical model describing the work function reduction in MXenes was developed in work [16]. This model proceeds from the fact that, in the general case, the variation of the work function under the influence of adsorbates deposited onto the surface is governed by three factors: a) a redistribution of the

electron charge between the surface and the adsorbates, b) adsorbate-induced surface relaxation, and c) the polarity of adsorbates [37]. MXenes on the basis of titanium and carbon layers – of the type that was first studied in work [34] (see Fig. 5) – which are most promising from the viewpoint of obtaining a low work function, were considered in work [16].

In the general case, non-terminated MXenes are mostly metals or semimetals (semiconductors with a zero band gap); a high value of the electron state density near the Fermi level in them is induced by external layers of transition metals (see work [36]). However, already in paper [34], it was experimentally shown that the termination of the Ti_3C_2 surface by hydroxyl groups leads to the appearance of a band gap of about 50 meV, and such MXene becomes a semiconductor.

Thus, the surface concentration of hydroxyl groups exceeds the concentration of charge carriers in this material. From Fig. 5, one can see that these hydroxyl groups form, on the surface, a monolayer with the same number of dipoles as the number of atoms in the transition-metal layer beneath. The band gap width exceeds an energy of 26 meV, which corresponds to the room temperature energy. Therefore, under normal conditions, every metal atom is related to less than one conduction electron. As a result, every dipole is associated with a negative electron charge localized near the oxygen atom and a positive one localized near the hydrogen atom. The terminalization shown in Fig. 5 is not accompanied by an appreciable rearrangement of the surficial Ti atoms. This means that the redistribution of the electron charge between the surface and the adsorbates, as well as the adsorbate-induced surface relaxation, can be neglected in the first approximation for a functionalized MXene on the basis of titanium and carbon. So, the work function reduction is mainly associated with the dipole moments of the hydroxyl OH groups.

In effect, the structure of energy levels that emerges at the boundary between the hydroxyl-group-terminated MXene and the vacuum is depicted in Fig. 3. Since the distance between the hydrogen and oxygen atoms in the hydroxyl group is $d = 0.97$ Å, this gap is transparent for the tunneling of thermal electrons located near the bottom of the conduction band in MXene (their wavelength is an order of magnitude larger), and they can freely tunnel from MXene into the vacuum. Therefore, the effective work function from MXene functionalized with hydroxyl groups is described by expressions (20) and (21), where N_s should be considered as the surface density of dipoles.

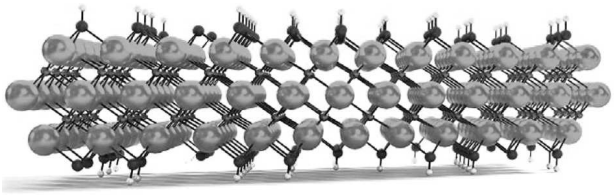

Fig. 5. First MXene structure $M_3X_2T_x$ [34] included three layers of transition metal (Ti) atoms (light large balls) and two layers of carbon (C) atoms between them (dark little balls), which were located between two termination planes composed of hydroxyl (OH) groups (oxygen atoms were located closer to and hydrogen atoms farther from metal atoms)

In work [16], for $N_s \approx 5 \times 10^{18}$ m^{-2}, $\varepsilon \approx 10$ (a dielectric constant value typical of semiconductors), and $d \approx 1 \times 10^{-10}$ m, the work function reduction was determined to be equal to about 3 eV. On the other hand, it was shown in work [12] that the work function in MXene non-functionalized with hydroxyl groups equals about 4.5 eV and practically does not depend on the number of Ti and C planes (varying from 1 to 9; the software packages used in work [12] allowed computations within the indicated interval). After the MXene functionalization, the work function decreases to approximately 1.6 eV and is also practically independent of the number of MXene planes [12].

At the same time, as was shown by calculations using the density functional method [38], for other MXene terminations, $Ti_3C_2T_x$, the work function values lie within an interval from 3.9 to 4.8 eV. A comparison with experimental data, which was carried out in the cited work, showed a substantial dependence of the work function on the surface composition.

Thus, the simple model proposed in work [16] can not only give a qualitative explanation to the considerable reduction of the work function in $Ti_{n+1}C_n$ with hydroxyl termination (which is visually illustrated in Fig. 3) but also demonstrates good quantitative agreement with the results of complicated and cumbersome numerical calculations from the first principles [12]. Therefore, this model can be used to evaluate the results of the functionalization of various MXene types with hydroxyl groups on the basis of the prospects of their application in emission electronics.

5. Experimental Methods for Determining the Work Function and the Electron Affinity

Consider various classes of experimental methods for measuring the work function and the electron affinity [39]. Since, as was indicated above, these parameters have a decisive influence on the electron emission from solids into vacuum, numerous methods of their experimental measurement are based exactly on various types of electron emission [40]. In metal specimens, electrons at the Fermi level can be excited and emitted into vacuum. By varying the excitation energy and measuring the electron emission parameters (the emission current density, the energy distribution of emitted electrons), the absolute value of the work function can be found. In practice, the thermal activation and photon absorption are used most often to excite electrons.

In the case of thermal activation of electron emission into vacuum, we deal with the ***thermionic emission method***. The basic working equation of the measuring technique is the Richardson–Dushman equation

$$J_S = AT^2 \exp\left(-\frac{\phi}{k_{\rm B}T}\right), \quad A = \frac{4\pi mek_{\rm B}^2}{h^3}. \tag{26}$$

This equation describes the dependence of the thermionic current density J_S on the temperature T and the work function ϕ. To determine the latter, the test specimen has to be under high-vacuum conditions and in contact with a thermostat maintaining a desired temperature of the specimen surface (Fig. 6). The measurement process consists in finding the current density J_S as a function of the temperature T. This procedure includes the measurement of the current in a circuit consisting of the test specimen (cathode), vacuum gap, anode, and voltage source, provided that there is no space charge in the vacuum near the specimen surface. In this case, the slope of the straight line representing the dependence of the quantity $\ln(J_S/T^2)$ on the inverse temperature is equal to $-\phi/k_{\rm B}$, which enables the experimental measurement of the work function of, e.g., refractory metals [41], carbon nanomaterials [42], borides [43], metal oxynitrides [44], and vanadates [45].

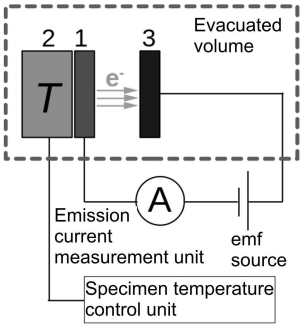

Fig. 6. Schematic diagram of the experimental setup for measuring the work function using the thermionic emission method: researched specimen (*1*), heater for maintaining a specimen temperature (*2*), anode (*3*)

Some errors may arise, because the Richardson–Dushman formula is based on the free-electron model, whereas the true dispersion law $E(\mathbf{k})$ may have substantial deviations from the simple quadratic dependence, and this formula for the emission current will not be absolutely accurate [46]. Let us recall that this dispersion law is nothing else but a set of eigenvalues $\varepsilon_{i\mathbf{k}}$ of the solutions of Eq. (4) obtained for a sufficient number of the wave vector values. It is also worth paying attention to the inapplicability of three-dimensional electron emission models to two-dimensional materials [47] and to the recent appearance of a modified Richardson–Dushman equation for two-dimensional materials, in particular, graphene and carbon nanotubes [48, 49]. Deviations from the Richardson–Dushman formula are also possible as a result of non-equilibrium effects [50].

Despite the apparent simplicity of the method described above, its practical implementation is not always possible, because the temperature required for the measurable emission current to appear may be too high, i.e., higher than the temperature of metal melting or the upper limit of the chemical compound stability. In this connection, the so-to-speak "reverse" scheme of the work function measurement using thermionic emission is applied, which is called the Anderson method [51, 52].

The essence of this method is that the examined specimen is an anode rather than a cathode. Electrons are emitted from a standard metallic thermionic cathode with a known (reference) work function. This cathode together with the test specimen (anode) forms a vacuum diode. The latter is connected to a circuit with a controllable constant voltage source and a measurement system that measures the current flowing through the diode (Fig. 7).

The thermionic cathode emits electrons, and the energies of the vast majority of them are concen-

trated immediately above the vacuum level of the cathode material. An important circumstance is that those electrons can be absorbed by the anode, only if their energies exceed the vacuum level of the anode material. Therefore, a current runs through the vacuum diode, only if the vacuum level of the cathode is equal to or higher than the vacuum level of the anode. In general, the vacuum levels in the cathode and anode differ from each other by the magnitude of the contact potential difference and the potential difference supplied from the external source. By changing the electromotive force of this source and measuring the current flowing through the diode as a function of the applied external voltage, it is possible to find the voltage value at which a transition takes place between the diode-on and diode-off operation modes. The found value, being multiplied by the elementary charge, just gives the difference between the sought work function and the reference work function of the cathode. If the reference value is known with high accuracy, then the entire procedure described above is equivalent to the measurement of the work function of the cathode material.

As an example, we can mention some recent works, where the Anderson method was used to measure the variation of the work function due to the adsorption of phthalocyanine molecules on the Ag(001) surface [53], or the coadsorption of Be and O on the Mo(112) surface [54–56], or the adsorption of Ce on the Mo(112) surface [9], or Be on the Mo(112) and Mo(011) surfaces [57], or Dy, Gd, and Sr on the Mo(112) surface [58, 59]. The ideas of the method were developed in combination with the methods of low-energy electron microscopy. As a result, there appeared a method for determining the work function with a lateral resolution in the specimen plane. Accordingly, the schematic diagram of the experiment (see Fig. 7) also includes an electron-optical system that creates an image of the examined surface with the help of electrons moving from the specimen.

As was indicated above, by varying the emf applied between the cathode and the specimen, it is possible to achieve the disappearance/appearance of an energy barrier prohibiting primary electrons from penetrating the specimen. In those cases, the surface image is formed by scattered/reflected electrons, respectively, and a transition between those regimes is accompanied by strong variations in the image brightness (this is an analog of the situation in the "ordinary" Anderson method, when the vacuum diode becomes open or closed).

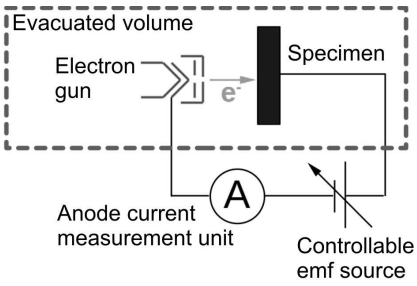

Fig. 7. Schematic diagram of the experimental setup for measuring the work function using the Anderson method

As an example, we mention microscopic studies of the work function of the eutectic mixture LaB_6/VB_2 [43]. It is interesting that the microscopic study of the work function of the specimen was also carried out in the cited paper using the thermionic emission method, i.e., as shown in Fig. 6, but including the electron-optical system of the surface image formation by low-energy electrons. It was done, because the image formation system was already included into the experimental scheme, and the specimen material allowed its non-destructive research in the thermionic mode.

Consider the excitation of the electron emission from a solid into vacuum with the help of photon absorption; in this case, we deal with photoelectron emission, and the work function is measured using the photoelectron spectroscopy (FES) method [60, 61]. The measurements are carried out under ultrahigh-vacuum conditions. The specimen is irradiated with monochromatic electromagnetic radiation with a quantum energy ranging from a few to several tens of electronvolts. The emitted photoelectrons get into an energy analyzer, which registers their distribution over the kinetic energy (Fig. 8). The energy scale of the analyzer is preliminary calibrated using an undoubtedly metallic specimen with a sharp Fermi edge. As a result, the determination of the maximum kinetic energy from the entire spectrum becomes easy. This energy corresponds to electrons emitted from specimen's Fermi level, which, in the equilibrium state, coincides with the Fermi level of the collector electrode in the energy analyzer.

Thus, the level $E_{k,\mathrm{Fermi}}$ corresponding to the kinetic energy of electrons emitted from the Fermi level becomes fixed on the kinetic energy scale of the en-

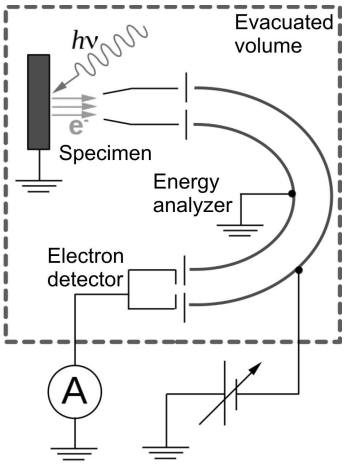

Fig. 8. Schematic diagram of the experimental setup for measuring the work function using the photoelectron spectroscopy method

ergy analyzer. Later on, when studying an unknown specimen, the work function of the latter is determined as the photon energy E_{photons} minus the difference between $E_{k,\text{Fermi}}$ and the minimum kinetic energy $E_{\min}$ of photoelectrons in the examined spectrum displayed on the calibrated energy scale of the spectrometer: $\Phi = E_{\text{photons}} - (E_{k,\text{Fermi}} - E_{\min})$.

More generally, the FES spectra demonstrate the density of occupied electronic states at the Fermi level and below, i.e., the states from which photoelectron emission is possible. In the case of a semiconductor, electrons mostly do not exist at the Fermi level, so electrons with the energy $E_{k,\text{Fermi}}$ are not emitted. As a result, the photoelectron spectrum has zero intensity at the Fermi level. Instead, the spectra demonstrate the existence of electrons with kinetic energies from a certain value that is lower than $E_{k,\text{Fermi}}$ and corresponds to the valence band top.

Here are the examples of how the FES method is applied to study semiconductors. In paper [62], the work function (4.04–6.4 eV), and position of the valence band top (1.2–3.44 eV) were measured in a promising semiconductor $ZnSnN_2$, and their dependences on the surface treatment method, the contamination level, and other factors were systematically investigated. FES is actively used to measure the work function of practical cathodes; for example, a substantial decrease in the work function of LaB_6 due to the adsorption of a BN monolayer was registered in work [63]. The results of a systematic FES study of the work function of the films consisting of a mixture of borides and nitrides of lanthanum, cerium, aluminum, and carbon can be found in work [64]; the lowest work function value is 2.8 eV. An interesting recent result is a rather low work function of about 2 eV measured for silver-potassium nanoparticles, which is a result of the formation of a surface alloy of those two metals [65].

For MXenes, the work function and the spectrum of occupied electronic states, as well as their dependences on the termination type, were also measured. For example, in work [66], a metallic character of conductivity and a rather high work function of 4.6 eV were found for MXenes $Ti_3C_2T_x$; the dependences of the structure of their valence band on the elemental composition and the atomic geometry of terminating groups were studied in detail in work [67]. Finally, with the help of the FES method, it was directly confirmed that the work function of MXene $Ti_3C_2T_x$ can be tunned within a very wide interval from 2.44 to 5.69 eV by functionalizing its surface with such molecules as 1,3,4,5,7,8-hexafluoro-11,11,12,12-tetracyanonaphtho-2,6-quinodimethane and (pentaethylcyclopentadienyl)(1,3,5-trimethylbenzene)ruthenium dimer [68].

Based on the fact that only occupied electronic states are engaged in the photoemission process, there arises a problem concerning the measurement of the electron affinity of semiconductors. It can be solved by applying an experimental technique that was termed the inverse photoelectron spectroscopy (IPES or IPS) [69, 70]. As one may guess from the name, a physical process is used that is inverse to photoelectron emission, namely, the capture of a free electron onto an unoccupied electronic state in the conduction band and the photon emission due to the release of the corresponding portion of energy (Fig. 9).

Two modes of IFS spectrum measurements are possible: (i) the measurement of the intensity of a flux of photons with a fixed energy as a function of the energy of electrons bombarding the specimen surface and (ii) the measurement of the spectrum of photons emitted by the specimen owing to its bombardment with electrons with a fixed kinetic energy. Typical energies of both electrons and photons can lie in an interval from a few to tens of electronvolts; the former case is distinguished as Low Energy Inverse Photoemission Spectroscopy (LEIPS) [71]. Low energies of electrons are an important factor that allows

a non-destructive analysis, in particular, of the films of organic molecules, for example, copper phthalocyanine (an electron affinity of 2.92 eV) [72]. There are works, where the same semiconductor specimen was studied using two methods, FES and IFS, in parallel. This combination made it possible to determine simultaneously the work function and the edges of the conduction and valence bands, i.e., the electron affinity and the band gap width; for instance, $\chi = 2.2$ eV and $E_g = 4.3$ eV for thin Eu_2O_3 films [73], $\chi = 4.03$ eV and $E_g = 2.16$ eV for thin C_{60} films [74], $E_g = 2.69$ eV for 8-cycloparaphenylene, $E_g = 3.29$ eV for 9-cycloparaphenylene, and $E_g = 3.33$ eV for 12-cycloparaphenylene [75].

Electrons can be emitted from solids into the vacuum not only over the potential barrier at the solid-vacuum interface, but also via their tunneling through it. Depending on how far from the surface the opposite electrode is located, the field and tunnel emissions are distinguished. If the opposite electrode (anode) is located sufficiently far, electrons tunnel through the barrier and move toward the anode in the vacuum as free particles; this is the field emission. If the opposite electrode is at a distance of a few tenths of a nanometer, an electron transits via the tunneling through the barrier from a certain bound state in the cathode material to another bound state in the anode material. This emission is called tunnel, and it serves as a basis for the determination of the electronic structure of both the valence and conduction bands; the method was called tunnel spectroscopy. This method is implemented in scanning probe microscopes, so it is often referred to as scanning tunneling spectroscopy (STS) [76, 77].

The STS method can be applied in a scanning tunneling microscope (STM) or an atomic force microscope (AFM) [76, 77]. In both cases, the key components of the experiment are the surface of the researched specimen and the pyramidal probe with a sufficiently small rounding radius of its apex (typically from an atomic radius to several tens of nanometers). In the operation mode, the main task of both STM and AFM is to maintain a constant distance between the surface and the probe apex (usually with the help of precision piezoelectric actuators).

In STM, the distance is controlled to maintain a constant tunnel current through the barrier at a constant voltage applied between the tip and the surface (Fig. 10). This operation mode is called the constant-current mode. Under all other identical conditions, a constant current is provided by the constant transparency of the tunnel barrier, which in the simplest approximation is achieved by maintaining a constant distance between the surface and the probe apex. After the stabilization of this distance at certain tunnel current and voltage values, it is fixed and remains constant during the measurement of the

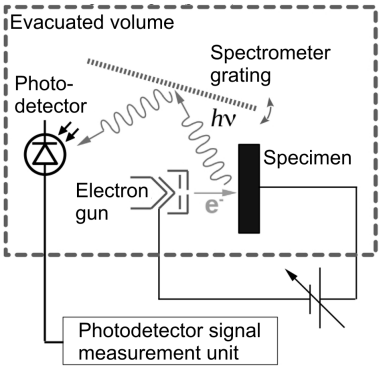

Fig. 9. Schematic diagram of the experimental setup for measuring the work function using the inverse photoemission spectroscopy method

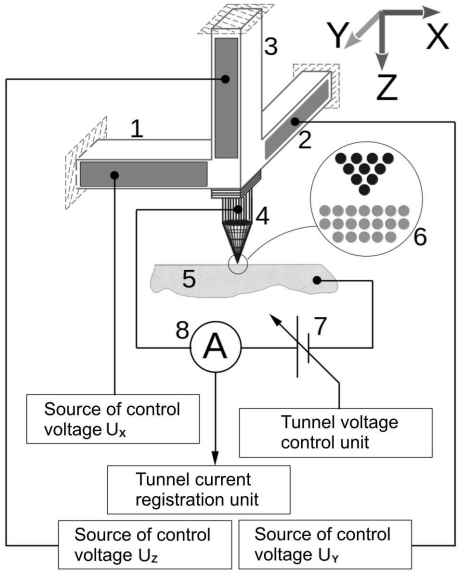

Fig. 10. Schematic diagram of scanning tunneling spectroscopy measurements in a scanning tunneling microscope: piezoelectric actuator along the X-axis (*1*), piezoelectric actuator along the Y-axis (*2*), piezoelectric actuator along the Z-axis (*3*), probe tip (*4*), specimen (*5*), magnified image of the probe-gap-specimen region (*6*), controllable source of tunnel voltage (*7*), tunnel current measurement unit (*8*)

current-voltage characteristic (CVC) of the formed tunnel contact. This process consists in an incremental variation of the tunnel voltage within a certain interval and the measurement of the tunnel current value at every discrete voltage value.

The specific feature of the measurement procedure of the tunnel contact CVC in the AFM consists in that the probe performs high-frequency (tens or hundreds of kHz) vibrations along the direction perpendicular to the researched surface plane. This is necessary for the functioning of the measurement system for the force acting between the probe and the surface. The minimum distance during one vibration period in the AFM can be of the same order of magnitude as the stationary distance between the probe and the surface in the STM. At other time moments during the vibration period, this distance is larger (depending on the vibration amplitude). This mode of AFM operation is called non-contact, because the probe never comes into mechanical contact with the surface. In this mode, the time-averaged value of the distance between the surface and the probe apex is maintained at a constant level corresponding to the average interaction force between them. As a result of distance oscillations, the transparency of the tunnel barrier also oscillates in time. So, if the tunnel voltage is constant, the tunnel current also oscillates. Nevertheless, the CVC measurement is possible, if the measurement time of one point of this characteristic – i.e., the time interval during which the tunnel voltage remains constant – exceeds the probe vibration period. The corresponding current value averaged over the vibration period determines every CVC point.

Thus, the main result of the measurements with the help of STM is the CVC of the tunnel contact created by the researched surface, the probe, and the vacuum gap between them. In practice, probes with distinctly pronounced metallic properties – i.e., with a Fermi level located in the conduction band and a sharp Fermi edge – are applied, as a rule. Let us consider how the positions of the valence band top and the conduction band bottom can be determined in this case, if the examined specimen is a semiconductor, and if its Fermi level is in the band gap. If the tunnel voltage between the specimen and the probe is zero, their Fermi levels coincide, the system is in equilibrium, and the tunnel current equals zero.

At a low non-zero positive voltage at the specimen with respect to the probe, the Fermi level in the specimen decreases with respect to that in the probe. However, although the tunneling barrier transparency is non-zero, electrons cannot tunnel from the probe into the specimen, because there are no electronic states in the energy interval between the two Fermi levels. The same situation takes place at a rather low negative voltage at the specimen with respect to the probe. So, if the tunnel voltage magnitude, irrespective of the voltage polarity, is rather small, a section with a zero current value is observed in the CVC. If the tunnel voltage magnitude grows, a non-zero tunnel current appears either at a positive voltage at the specimen, when the conduction band bottom in the semiconductor reaches the Fermi level in the probe, or at a negative voltage at the specimen, when the valence band top reaches the Fermi level in the probe. From the aforesaid, it is possible to draw the following general conclusion about the CVC shape in the considered experimental situation. At low tunnel voltages, there exists a zero-current interval whose width is equal to the band gap width in the semiconductor. Beyond this interval, the tunnel current becomes non-zero and, as a rule, increases with the growth of the tunnel voltage magnitude. The positive voltage value at which the current starts to grow from zero equals to the energy of the conduction band bottom reckoned from the Fermi level. Analogously, the negative voltage value at which the current starts to decrease from zero is equal to the energy of the valence band top reckoned from the Fermi level. For a more precise determination of those energies, STS experiments are often carried out at cryogenic temperatures of the specimen and the probe [78], because the narrower width of the Fermi step reduces the smearing of the transition between the zero and non-zero tunnel current intervals in the CVC.

An advantage of STS over FES and OFES is that the edge positions and the structures of the valence and conduction bands can be determined in the same experiment. For example, in work [79], using the STS method, the positions of the band edges in $CsPbBr_3$ were measured to equal -1 and $+1.5$ eV, and they were compared with the results obtained by FES, OFES, and calculations in the framework of the density functional theory. Furthermore, STS has an extremely high (at the atomic level) spatial resolution in the specimen surface plane, which allows the positions of band edges to be locally measured at heterogeneous surfaces and in nano-objects. For example,

in work [80], a series of tunnel spectra were obtained for the surfaces of cadmium selenide nanoplates with various thicknesses; the band edges of about −1 and +1 V were determined for a thickness of 7 monolayers, and the expansion of the band gap with the decreasing thickness was revealed. The band edges were registered at −0.09 and +0.1 eV in graphene nanoribbons with a width of 17 atoms, and at −0.06 and +1.28 eV in 13-atom-width nanoribbons [81].

Nanoscale monolayer islands of tellurene were studied in work [82]. In particular, the band edges in them were registered at −0.41 and +0.53 eV, as well as the absence of a forbidden band on their periphery, in full agreement with the theoretical prediction of the state of topological insulator for this two-dimensional material.

STS is also a convenient tool for studying the electronic structure evolution at the transition between two- and three-dimensional allotropes. In particular, it was shown for indium nitride that the band gap in this two-dimensional material equals 2 eV, whereas it is 0.7 eV in the bulk InN specimen [83]. In work [84], using the STS method, the band edges were measured at the positions of −1.77 and +0.86 eV in one-monolayer MoS_2, and at −1.24 and +0.63 eV in two-monolayer MoS_2.

Besides the direct application of the STS technique, equivalent information about the energy location of the band edges can be obtained with the help of the voltage-dependent STM method, which consists in obtaining a series of images of the same surface area at various tunnel voltages. This method was used in works [85, 86] to detect the semiconducting character of two-dimensional bismuth adsorbates, which did not form a continuous film on the Ge(111) surface, and determine the edge position of their conduction band (0.5 eV above the Fermi level in the germanium substrate.

The STS technique allows the positions of the band edges to be measured with respect to the Fermi level. However, this is not enough to determine the electron affinity. This task requires an independent measurement of the Fermi level position with respect to the vacuum level, i.e., the work function. To solve this problem with the help of scanning probe microscopy, the most suitable method is the scanning Kelvin probe microscopy (SKPM) [87]. The SKPM is implemented making use of an AFM operating in the non-contact mode. In the SKPM experiment, the

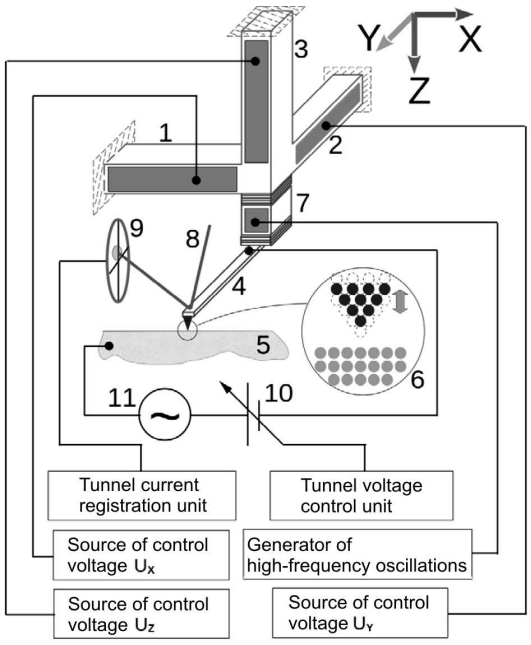

Fig. 11. Schematic diagram of scanning Kelvin probe microscopy: piezoelectric actuator along the X-axis (*1*), piezoelectric actuator along the Y-axis (*2*), piezoelectric actuator along the Z-axis (*3*), elastic element (cantilever) with a fastened probe (*4*), specimen (*5*), magnified image of the probe-gap-specimen region (*6*), high-frequency piezoelectric actuator along the Z-axis (*7*), laser beam (*8*), position-sensitive photodetector (*9*), controllable source of constant compensating voltage (*10*), source of alternating voltage between the tip and the specimen (*11*)

standard AFM equipment is complemented with a controllable source of constant voltage and a source of harmonic alternating voltage with a frequency far (as a rule lower) from the frequency of probe vibrations with respect to the specimen surface, as well as a synchronous AC voltage detector and a special feedback circuit. Both sources are connected in series between the specimen and the probe (Fig. 11).

If the specimen and probe bulks are connected by an electrical conductor, then their electronic subsystems are in equilibrium, and the Fermi levels coincide. At the same time, if the work functions of the specimen and the probe differ from each other, there arises a contact potential difference (CPD) between their surfaces. In essence, the specimen and the probe are the plates of a capacitor charged to the corresponding voltage, and there is an electrostatic attractive force between them, which depends on the instantaneous voltage value across the capacitor. As a result, there

arises a force between the specimen and the probe, which oscillates with the frequency of applied alternating voltage and has an amplitude proportional to the sum of the CPD and the constant voltage of the controlled source.

Since the AFM probe is mechanically fastened to the end of an elastic element (the cantilever), the probe vibrates at the frequency of the applied alternating voltage. Those vibrations occur simultaneously with the cantilever vibrations at the same frequency that are used to stabilize the average distance between the probe and the specimen. The amplitude of the cantilever and, therefore, the probe vibrations is determined with the help of a laser beam that is reflected from it and falls on a position-sensitive photodetector. Supplying the signal from the photodetector to a suitable synchronous detector, the measured vibration amplitude at the frequency of the alternating voltage source can be obtained. The corresponding signal is sent to a special feedback circuit that adjusts the controllable source of constant voltage until the cantilever vibrations reach zero amplitude.

Since this amplitude is proportional to the sum of the CPD and the instantaneous voltage value of the controllable source, the zeroing of the cantilever vibration amplitude at the frequency of the AC voltage source is attained, if the voltage of the controllable source is exactly opposite to that of CPD. Thus, by reading our the voltage of the controlled source, which was installed in the SKPM experiment, and finding its sign, we obtain a CPD value between the specimen and the probe, which is characteristic of the specimen surface point above which the probe tip is located. The CPD is the difference between the work functions of the specimen and the probe; so, knowing the work function of the probe, it is possible to determine the work function of the specimen. But if the work function of the probe material is not exactly known, an additional measurement can be carried out making use of a reference specimen with the precisely known work function. Afterward, the unknown work functions of other studied specimens can be measured provided that the same probe in the same state is used [88, 89].

The SKPM technique was used to measure the work function Φ of many homogeneous and heterogeneous surfaces and nano-objects. For titanium oxide (TiO) nanowires with an atomically clean surface, the value $\Phi = 3.31$ eV was obtained, and a work function growth due to the contact with the atmosphere was registered [90]. The value $\Phi = 4.28$ eV was found for MXene $Ti_3C_2T_x$ [91]. For two-dimensional materials on the basis of copper iodide and ligands, $\Phi = 5.46$ eV (2D-CuI$(pm)_{0.5}$) and 5.26 eV (2D-CuI$(pz)_{0.5}$) [92]. For MoS_2 nanolayers, a work function value of 4.53 eV was obtained, as well as the distribution maps of the work function deviations from the average value over the surface plane. It was found that this distribution changes after the surface bombardment with high-energy argon ions [93]. It is worth noting that the Kelvin probe can also be used for the measurement of the work function in a non-microscopic variant, i.e., without scanning the surface and obtaining its image. An example is the measurement of the work function of Os–Ru–W thin films and its dependence on the W concentration [94].

6. Experimental Techniques for Obtaining Surfaces with Low Work Function

Let us consider modern experimental approaches to reducing the work function and the electron affinity of the metal and semiconductor surfaces. As a result of the surface treatment carried out in the framework of such approaches, a spatial separation of electric charges in the direction perpendicular to the surface plane has to be created in the near-surface region of the specimen. This state can be characterized by the spatial distribution along this direction of the positive and negative charges localized either in two different atomic planes or in one atomic plane and an extended space region, the latter case being usually typical of semiconductor substrates. The production technologies of such surfaces can be based on various methods of adsorbate deposition on the metal or semiconductor surface: physical vapor deposition, chemical vapor deposition, deposition from the liquid phase, diffusion from the substrate bulk, and others.

Conceptually, the simplest is the surface adsorption of a layer of molecules or molecular groups that are characterized by their own (intrinsic) dipole moment in the absence of an external electric field. At the same time, in order to achieve the desired effect, it is necessary to provide an identical (and favorable from the viewpoint of the work function reduction) orientation of all adsorbed molecules. Such a situation is realized in a natural way in self-assembled mono-

layers (SAMs). For example, a monolayer of pyridine molecules is adsorbed on the ZnO(1010) surface in an ordered manner, with all molecules being oriented identically, which decreases the work function by 2.9 eV [95]. In work [96], some biphenyl-based molecules with phosphine groups were synthesized; the latter provided a fixed attachment point to the substrate. Two types of molecules had a polar pyrimidine group with the dipole moment vector directed to/from the phosphine group, i.e., to/from the substrate in the formed monomolecular layer. The molecules of the third type were non-polar. As a result of the self-assembling of the monolayers of those three types of molecules on the indium tin oxide (ITO) substrate, the corresponding work function values were registered: 3.9 eV (the molecular dipole moments are directed to the surface), 4.85 eV (from the surface), and 4.4 eV (along the surface). In the summarizing work [97], a universal recipe for reducing the work function of metals, optically transparent and electrically conductive metal oxides, electrically conductive polymers, and graphene by more than 1 eV by depositing polyethyleneimine ethoxylate or branched polyethyleneimine films on their surfaces was proposed.

The concept of adsorbed dipole molecules can also include bilayer structures, where each layer consists of identical molecules (but the molecules are different for each layer) and makes its contribution to the reduction of the work function. In particular, in work [98], a reduction of the work function was found for a large number of oxides (without any exception) after the contact of their initially atomically clean surface with the ordinary atmosphere. As a result of this contact, there emerged an adsorbed double "sandwich" consisting of an OH layer adjacent to the oxide surface and an H_2O layer above. Hydrogen bonds were formed between the OH and H_2O layers, and their dipole moments were oriented in tandem, which resulted in a reduction of the surface work function. Another conceptual approach is the coadsorption of metal atoms (including the atoms of mixtures of various metals) and oxygen atoms, which is the standard activation method of thermionic cathodes [99]. A surface dipole layer is formed by negatively charged oxygen ions located closer to the substrate and positively charged metal ions located further from the substrate. In the framework of this concept (simply, a theoretical model developed in detail in works [14, 15]), the already mentioned experiments [8] on the coadsorption of gadolinium and oxygen on a silicon substrate were performed, where a work function value below 1 eV was reached. This concept turned out applicable to advanced two-dimensional materials. For instance, a reduction of the graphene work function to a record value of 1.01 eV (!) was obtained in work [100] by coating graphene with a mixture of cesium and oxygen atoms.

Among the novel carbon materials, the most convenient from the viewpoint of cathode applications are carbon nanotubes. By coating them with a mixture of barium, strontium, and oxygen, a work function value of 1.6 eV was achieved, whereas the nanotube morphology enhanced the electric field strength at emitting surfaces [101]. Coating the diamond (100) and (111) surfaces with a mixture of aluminum and oxygen atoms led to negative values of electron affinity (up to -1.0 eV) and a work function from 4 to 5 eV [102]. The deposition of sub-monolayer amounts of titanium on an oxidized diamond (100) surface gave a negative electron affinity value of -0.7 eV [103]. Its record value (-2.01 eV) was obtained on the diamond (100) surface by coating it with a mixture of magnesium and oxygen atoms [5].

This approach also allows a simultaneous application of metal atoms of two types. For instance, the coating of the same diamond surface with a SnO layer intercalated with lithium resulted in a 2.3-eV work function reduction [104]. A record low value of the work function (0.7 eV) was obtained for n-GaAs via the cesium and oxygen adsorption on its surface subjected to external lighting at a wavelength of 532 nm, which led to the generation of surface photo-emf [105].

The work function or the electron affinity can also be decreased by adsorbing only one type of atoms on the substrate surface. In this case, the positive charge is concentrated in the plane, where the adsorbed atoms are located, whereas the negative charge can be either concentrated in the external atomic layer of the substrate or continuously distributed into the substrate depth. In the already mentioned work [9], the adsorption of cerium on a single-crystalline substrate Mo(112) resulted in a reduction of the work function by 2.2 eV. In work [106], a decrease in the work function of the Pt(111) surface was registered after its contamination with carbon, with a linear dependence of the work function reduction on the sur-

face concentration of carbon atoms. In work [107], a negative electron affinity of −1.38 eV was achieved on the (111) surface of p-doped diamond terminated with a layer of hydrogen atoms. The negative values of the electron affinity of diamond obtained due to the adsorption on its surface of some metals in amounts to one monolayer can be found in work [108].

One more concept consists in a specific treatment of the surface giving rise to the creation of defects in the near-surface crystal lattice; these can be vacancies or inclusions of foreign atoms, and so forth. Such centers can be charged, or they can play the role of traps that can capture charge carriers from the bulk. As an example, the dependence of the work function of the oxides of transition metals (Cu, Mo, Ni, V, Ti, W, Cr, Ta, Co) on the surface concentration of oxygen vacancies can be used, which was plotted on the basis of experimental FES measurements: a monotonous decrease of the work function value with the increase of the concentration of such vacancies [109]. In work [110], a graphite surface was sequentially treated with hydrogen and nitrogen plasmas, which stimulated the formation of surface carbon vacancies and inclusions of individual nitrogen atoms. As a result, a reduction of the work function to 2.9 eV was obtained. In the case of two-dimensional material, the surface treatment is simultaneously the treatment of the material bulk. In particular, a systematic study of graphene interaction with a large number of molecular reagents was carried out [111]. As a result, graphene was doped to various types and levels, and the variations of its work function were experimentally registered.

A review of experimental works, where all abovementioned and some other specific approaches were used to obtain a diamond surface with a negative electron affinity can be found in work [6].

7. Conclusions

Intense efforts were applied to create metal surfaces with a low work function and semiconductor and insulator surfaces with a low/negative electron affinity. However, such works require the development of simple intuitive theoretical models that would allow the affinity values to be evaluated, at least preliminarily, rather simply, without applying cumbersome calculations on the basis of the Kohn–Sham equations.

In work [14], in the framework of a developed simple intuitive model, it was shown that the presence of a dipole layer (e.g., from negatively charged oxygen atoms and positively charged rare earth metal atoms) with equal concentrations of differently charged adsorbed atoms on the semiconductor surface can lead to a reduction of the electron affinity by up to 3 eV. In work [15], it is shown that the asymmetry between the surface concentrations of oxygen and metal atoms can lead to two opposite consequences: if the negatively charged oxygens prevail, a decrease in the electron affinity becomes smaller due to the upward band bending in the SCR of a semiconductor, and if the positively charged metal atoms prevail, a decrease in the electron affinity becomes larger due to the downward band bending. This result allows the proposition of technological solutions for obtaining the surfaces with a minimum work function for modern electron emission devices.

In work [16] in the framework of a simple developed theoretical model, the work function value was estimated for MXene functionalized with hydroxyl groups. In the non-functionalized material, it is equal to about 4.5 eV and practically does not depend on the number of Ti and C planes (varying from 1 to 9). After the functionalization, it decreases to about 1.6 eV and remains practically independent of the number of MXene planes.

Intense searches are carried out for the development of reliable experimental methods aimed at obtaining the low work function values of various surfaces that can be used in electron emission devices. The surface treatment in the framework of the applied approaches should result in the creation of a spatial separation of electric charges in the near-surface specimen region in the direction perpendicular to the surface plane. This state can be characterized by spatial distributions of positive and negative charges along this direction, with their localization either in two different atomic planes or in one atomic plane and an extended space region (the latter variant is typical of semiconductor substrates). Technologies for obtaining such surfaces can be based on various methods of deposition of adsorbates on the metal or semiconductor surface: physical vapor deposition, chemical vapor deposition, deposition from the liquid phase, diffusion from the substrate bulk, and others.

Various methods of obtaining the diamond surface make it possible to achieve large negative values of the electron affinity. A record negative value of −2.01 eV was obtained on the diamond (100) sur-

face coated with a mixture of magnesium and oxygen atoms [5, 6]. However, searches for reliable and reproducible methods for obtaining the low work function or electron affinity values for metal or semiconductor cathodes (unlike diamond, they can provide a high rate of supply of emitted carriers to the surface through the bulk) go on further.

Currently, the search is performed for the ways aimed at developing the cathodes based on, e.g., the adsorption of alkaline and rare earth (Ce, Gd, Eu) metals and the oxygen coadsorption on the Si, Ge, and Mo surfaces (in the nanostructured state as well), where charge double layers can be formed, which substantially reduces the work function [8, 9].

The authors are grateful to Taras Shevchenko National University of Kyiv for supporting this work.

1. W.E. Spicer, A. Herrera-Gomes. Modern theory and applications of photocathodes. *Proc. SPIE* **2022**, 18 (1993).
2. A. Evtukh, H. Hartnagel, O. Yilmazoglu, H. Mimura, D. Pavlidis. *Vacuum Nanoelectronic Devices: Novel Electron Sources and Applications* (John Wiley and Sons, 2015).
3. Y. Zhou, P. Zhang. Theory of field emission from dielectric coated surfaces. *Phys. Rev. Res.* **2,** 043439 (2020).
4. N.D. Lang, W. Kohn. Theory of metal surfaces: Work function. *Phys. Rev. B* **3,** 1215 (1971).
5. K.M. O'Donnell, M.T. Edmonds, A. Tadich, L. Thomsen, A. Stacey, A. Schenk, C.I. Pakes, L. Ley. Extremely high negative electron affinity of diamond via magnesium adsorption. *Phys. Rev. B* **92**, 035303 (2015).
6. M.C. James, F. Fogarty, R. Zulkharnay, N.A. Fox, P.W. May. A review of surface functionalisation of diamond for thermionic emission applications. *Carbon* **171**, 532 (2021).
7. R.Calish. Doping of diamond. *Carbon* **37**, 781 (1999).
8. M.G. Nakhodkin, M.I. Fedorchenko. Interaction of oxygen and gadolinium with Si(100)-2×1. Formation of a system with a work function of 1 eV. *Ukr. J. Phys.* **60**, 97 (2015).
9. T.V. Afanasieva, A.G. Fedorus, A.M. Goriachko, A.G. Naumovets, I.M. Neporozhnii, D.V. Rumiantseva. Mesoscopic self-ordering in oxygen doped Ce films adsorbed on Mo(112). *Surf. Sci.* **705**, 121766 (2021).
10. H.A. Tahini, X. Tan, S.C. Smith. The origin of low work-functions in OH terminated MXenes. *Nanoscale* **9**, 7016 (2017).
11. F. Maier, J. Ristein, L. Ley. Electron affinity of plasma-hydrogenated and chemically oxidized diamond (100) surfaces. *Phys. Rev. B* **64**, 165411 (2001).
12. M. Khazaei, M. Arai, T. Sasaki, A. Ranjbar, Y. Liang, S. Yunoki. OH-terminated two-dimensional transition metal carbides and nitrides as ultralow work function materials. *Phys. Rev. B* **92**, 075411 (2015).
13. E. Zojer, T.C. Taucher, O.T. Hofmann. The impact of dipolar layers on the electronic properties of organic/inorganic hybrid interfaces. *Adv. Mater. Interfac.* **6**, 1900581 (2019).
14. M.V. Strikha, A.M. Goriachko. A theoretical model for describing a reduction of the work function for a semiconductor/insulator under the influence of the surface charge double layer. *Sensor. Elektron. Mikrosyst. Tekhnol.* **19** (3), 23 (2022) (in Ukrainian).
15. M.V. Strikha, D.V. Antonyuk. Influence of adsorbed monolayers with an arbitrary concentration ratio between opposite charges on the electron affinity of semiconductor. *Sensor. Elektron. Mikrosyst. Tekhnol.* **20** (1), 4 (2023) (in Ukrainian).
16. M.V. Strikha, D.V. Antonyuk A theoretical model for estimating the work function of MXenes with hydroxyl termination. *Fiz. Khim. Tverd. Tila* **23** (1), 102 (2023) (in Ukrainian).
17. S. Halas, T. Durakiewicz. Is work function a surface or a bulk property? *Vacuum* **85**, 486 (2010).
18. A. Kahn. Fermi level, work function and vacuum level. *Mater. Horiz.* **3**, 7 (2016).
19. M. Yoshitake. *Work Function and Band Alignment of Electrode Materials* (Springer Japan KK, 2021).
20. Ye.S. Kryachko, Ye.Yu. Remeta. Density functional theory in atomic physics. *Ukr. J. Phys.* **9,** 38 (2014).
21. W. Kohn, L.J. Sham. Self-consistent equations including exchange and correlation effects. *Phys. Rev.* **140**, A1133 (1965).
22. F. Giustino. *Materials Modelling using Density Functional Theory* (Oxford University Press, 2014).
23. R. Jacobs, D. Morgan, J. Booske. Work function and surface stability of tungsten-based thermionic electron emission cathodes. *APL Materials* **5**, 116105 (2017).
24. S. Kim, M.Y. Lee, S. Lee, S.-H. Jhi. Super low work function of alkali-metal-adsorbed transition metal dichalcogenides. *J. Phys.: Condens. Matter* **29**, 315702 (2017).
25. R. Tran, X.-G. Li, J.H. Montoya, D. Winston, K.A. Persson, S.P. Ong. Anisotropic work function of elemental crystals. *Surf. Sci.* **687**, 48 (2019).
26. R.I.G. Hughes. Theoretical practice: the Bohm-Pines quartet. *Perspect. Sci.* **14**, 457 (2006).
27. N.D. Lang, W. Kohn. Theory of metal surfaces: Charge density and surface energy. *Phys. Rev. B* **1**, 4555 (1970).
28. I. Brodie, S.H. Chou, H. Yuan. A general phenomenological model for work function. *Surf. Sci.* **625**, 112 (2014).
29. S.H. Chou, J. Voss, I. Bargatin, A. Vojvodic, R.T. Howe, F. Abild-Pedersen. Orbital-overlap model for minimal work functions of cesiated metal surfaces. *J. Phys. Condens. Matter.* **24**, 445007 (2012).
30. G.P. Peka, V.I. Strikha. *Surface and Contact Phenomena in Semiconductors* (Lybid', 1992) (in Ukrainian).
31. V.A. Smyntyna. *Physico-Chemical Phenomena at the Solid Surface* (Astroprynt, 2009) (in Ukrainian).
32. R.J. Nemanich, P.K. Baumann, M.C. Benjamin, O.-H. Nam, A.T. Sowers, B.L. Ward, H. Ade, R.F. Davis.

Electron emission properties of crystalline diamond and III-nitride surfaces. *Appl. Surf. Sci.* **130–132**, 694 (1998).
33. A.M. Goriachko, M.V. Strikha. Nanostructured SiC as a promising material for the cold electron emitters. *Semicond. Phys. Quant. Electron. Optoelectron.* **24**, 355 (2021).
34. M. Naguib, M. Kurtoglu, V. Presser, J. Lu, J. Niu, M. Heon, L. Hultman, Y. Gogotsi, M. W Barsoum. Two-dimensional nanocrystals produced by exfoliation of Ti_3AlC_2. *Adv. Mater.* **23**, 4248 (2011).
35. M.D. Firouzjaei, M. Karimiziarani, H. Moradkhani, M. Elliott, B. Anasori. MXenes: The two-dimensional influencers. *Mater. Today Adv.* **13**, 100202 (2022).
36. X. Jiang, A.V. Kuklin, A. Baev, Y. Ge, H. Ågren, H. Zhang, P.N. Prasad. Two-dimensional MXenes: From morphological to optical, electric, and magnetic properties and applications. *Phys. Rep.* **848**, 1 (2020).
37. T.C. Leung, C.L. Kao, W.S. Su, Y.J. Feng, C.T. Chan. Relationship between surface dipole, work function and charge transfer: Some exceptions to an established rule. *Phys. Rev. B* **68**, 195408 (2003).
38. T. Schultz, N.C. Frey, K. Hantanasirisakul, S. Park, S.J. May, V.B. Shenoy, Y. Gogotsi, N. Koch. Surface termination dependent work function and electronic properties of $Ti_3C_2T_x$ Mxene. *Chem. Mater.* **31**, 6590 (2019).
39. O.C. Olawole, D.K. De, O.F. Olawole, R. Lamba, E.S. Joel, S.O. Oyedepo, A.A. Ajayi, O.A. Adegbite, F.I. Ezema, S. Naghdi, T.D. Olawole, O.O. Obembe, K.O. Oguniran. Progress in the experimental and computational methods of work function evaluation of materials: A review. *Helyon* **8**, e11030 (2022).
40. K.L. Jensen. *Introduction to the Physics of Electron Emission* (John Wiley & Sons, Ltd., 2018).
41. P.D. Swartzentruber, T.J. Balka, M.P. Effgenb. Correlation between microstructure and thermionic electron emission from Os–Ru thin films on dispenser cathodes. *J. Vac. Sci. Technol. A* **32**, 040601 (2014).
42. A. Sherehiy, S. Dumpala, A. Safir, D. Mudd, I. Arnold, R.W. Cohn, M.K. Sunkara, G.U. Sumanasekera. Thermionic emission properties and the work function determination of arrays of conical carbon nanotubes. *Diamond Rel. Mater.* **34**, 1 (2013).
43. T.C. Back, A.K. Schmid, S.B. Fairchild, J.J. Boeckl, M. Cahay, F. Derkink, G. Chen, A. Sayir. Work function characterization of directionally solidified LaB_6–VB_2 eutectic. *Ultramicroscopy* **183**, 67 (2017).
44. A. Bellucci, S. Orlando, M. Girolami, M. Mastellone, V. Serpente, B. Paci, A. Generosi, A. Mezzi, S. Kaciulis, R. Polini, D.M. Trucchi. Aluminum (Oxy)nitride thin films grown by fs-PLD as electron emitters for thermionic applications. *AIP Conf. Proc.* **2416**, 020004 (2021).
45. L. Lin, R. Jacobs, D. Chen, V. Vlahos, O. Lu-Steffes, J.A. Alonso, D. Morgan, J. Booske. Demonstration of low work function perovskite SrVO3 using thermionic electron emission. *Adv. Funct. Mater.* **32**, 2203703 (2022).
46. Y.C. Gerstenmaier, G. Wachutka. Thermionic emission laws for general electron dispersion relations and band structure data. *J. Appl. Phys.* **125**, 215105 (2019).
47. Y.S. Ang, L. Cao, L.K. Ang. Physics of electron emission and injection in two-dimensional materials: Theory and simulation. *InfoMat* **3**, 502 (2021).
48. D.K. De, O.C. Olawole. A three-dimensional model for thermionic emission from graphene and carbon nanotube. *J. Phys. Commun.* **3**, 015004 (2019).
49. O.C. Olawole, D.K. De, S.O. Oyedepo, F.I. Ezema. Mathematical models for thermionic emission current density of graphene emitter. *Sci. Rep.* **11**, 22503 (2021).
50. J.L. Domenech-Garret, S.P. Tierno, L. Conde. Non-equilibrium thermionic electron emission for metals at high temperatures. *J. Appl. Phys.* **118**, 074904 (2015).
51. P.A. Andreson. A new technique for preparing monocrystalline metal surfaces for work function study. The work function of Ag(100). *Phys. Rev.* **59**, 1034 (1941).
52. A. Sabik, F. Gołek, G. Antczak. Note: Work function change measurement via improved Anderson method. *Rev. Sci. Instrum.* **86**, 056111 (2015).
53. T. Wagner, G. Antczak, M. Györök, A. Sabik, A. Volokitina, F. Gołek, P. Zeppenfeld. Attenuation of photoelectron emission by a single organic layer. *ACS Appl. Mater. Interf.* **14**, 23983 (2022).
54. T. Afanasieva, A.G. Fedorus, A.G. Naumovets, D. Rumiantsev. Coadsorbed oligolayers of beryllium and oxygen on molybdenum (112) surface: Formation and chemical composition, atomic structure and evaporation. *Surf. Sci.* **682**, 14 (2019).
55. T. Afanasieva, A.G. Fedorus, D. Rumiantsev, I.N. Yakovkin. Honeycomb BeO monolayer on the Mo(112) surface: LEED and DFT study. *Appl. Surf. Sci.* **428**, 815 (2018).
56. A.G. Fedorus, A.A. Mitryaev, A.G. Naumovets. Interaction of oxygen with submonolayer beryllium films on Mo(112). *Eur. Phys. J. Appl. Phys.* **68**, 21302 (2014).
57. A.G. Fedorus, A.A. Mitryaev, A.G. Naumovets. Beryllium overlayers on Mo(112) and Mo(011) surfaces. *Surf. Sci.* **606**, 580 (2012).
58. A.A. Mitryaev, A.G. Naumovets, A.G. Fedorus. Surface alloy formation and two-dimensional vitrification in adsorbed monolayers on molybdenum (112) surfaces. *Low Temp. Phys.* **36**, 677 (2010).
59. A.G. Fedorus, A.A. Mitryaev, A.G. Naumovets. Irreversible structure transitions in Gd monolayers on Mo(112). *Eur. Phys. J. B* **71**, 47 (2009).
60. J.W. Kim, A. Kim. Absolute work function measurement by using photoelectron spectroscopy. *Curr. Appl. Phys.* **31**, 52 (2021).
61. J.E. Whitten. Ultraviolet photoelectron spectroscopy: Practical aspects and best practices. *Appl. Surf. Sci. Adv.* **13**, 100384 (2023).
62. A.M. Shing, Y. Tolstova, N.S. Lewis, H.A. Atwater. Effects of surface condition on the work function and valence-band position of $ZnSnN_2$. *Appl. Phys. A* **123**, 735 (2017).

63. H. Yamaguchi, R. Yusa, G. Wang, M.T. Pettes, F. Liu, Y. Tsuda, A. Yoshigoe, T. Abukawa, N.A. Moody, S. Ogawa. Work function lowering of LaB_6 by monolayer hexagonal boron nitride coating for improved photo- and thermionic-cathodes. *Appl. Phys. Lett.* **122**, 141901 (2023).
64. A. Mezzi, P. Soltani, S. Kaciulis, A. Bellucci, M. Girolami, M. Mastellone, D.M. Trucchi. Investigation of work function and chemical composition of thin films of borides and nitrides. *Surf. Interf. Anal.* **50**, 1138 (2018).
65. M.-H. Mikkelä, K. Jänkälä, M. Huttula, O. Björneholm, M. Tchaplyguine. Free silver nanoparticles doped by potassium: Work-function change in experiment and theory. *J. Chem. Phys.* **154**, 234708 (2021).
66. E. Aydin, J.K. El-Demellawi, E. Yarali, F. Aljamaan, S. Sansoni, A. Rehman, G. Harrison, J. Kang, A. El Labban, M. De Bastiani, A. Razzaq, E. Van Kerschaver, T.G. Allen, O.F. Mohammed, T. Anthopoulos, H.N. Alshareef, S. De Wolf. Scaled deposition of $Ti_3C_2T_x$ MXene on complex surfaces: Application assessment as rear electrodes for silicon heterojunction solar cells. *ACS Nano* **16**, 2419 (2022).
67. L.-Å. Näslund, M.-H. Mikkelä, E. Kokkonen, M. Magnuson. Chemical bonding of termination species in 2D carbides investigated through valence band UPS/XPS of $Ti_3C_2T_x$ Mxene. *2D Materials* **8**, 045026 (2021).
68. T. Schultz, P. Bärmann, E. Longhi, R. Meena, Y. Geerts, Y. Gogotsi, S. Barlow, S.R. Marder, T. Petit, N. Koch. Work function and energy level alignment tuning at $Ti_3C_2T_x$ MXene surfaces and interfaces using (metal-)organic donor/acceptor molecules. *Phys. Rev. Mater.* **7**, 045002 (2023).
69. V. Dose. VUV isochromat spectroscopy. *Appl. Phys.* **14**, 117 (1977).
70. H. Yoshida. Principle and application of low energy inverse photoemission spectroscopy: A new method for measuring unoccupied states of organic semiconductors. *J. Electr. Spectrosc. Rel. Phenom.* **204**, 116 (2015).
71. H. Yoshida. Note: Low energy inverse photoemission spectroscopy apparatus. *Rev. Sci. Instrum.* **85**, 016101 (2014).
72. H. Yoshida. Near-ultraviolet inverse photoemission spectroscopy using ultra-low energy electrons. *Chem. Phys. Lett.* **539–540**, 180 (2012).
73. T. Hadamek, S. Rangan, J. Viereck, D. Shin, A.B. Posadas, R.A. Bartynski, A.A. Demkov. Stoichiometry, band alignment, and electronic structure of Eu_2O_3 thin films studied by direct and inverse photoemission: A reevaluation of the electronic band structure. *J. Appl. Phys.* **127**, 074101 (2020).
74. M. Terashima, T. Miyayama, T. Shirao, H.W. Mo, Y. Hatae, H. Fujimoto, K. Watanabe. The electronic band structure analysis of OLED device by means of in situ LEIPS and UPS combined with GCIB. *Surf. Interf. Anal.* **1**, 5 (2020).
75. K. Kanai, T. Inoue, T. Furuichi, K. Shinoda, T. Iwahashi, Y. Ouchi. Electronic structure of n-cycloparaphenylenes directly observed by photoemission spectroscopy. *Phys. Chem. Chem. Phys.* **23**, 8361 (2021).
76. B. Voigtländer. *Scanning Probe Microscopy – Atomic Force Microscopy and Scanning Tunneling Microscopy* (Springer-Verlag, 2015).
77. E. Meyer, R. Bennewitz, H.J. Hug. *Scanning Probe Microscopy – The Lab on a Tip* (Springer Nature Switzerland AG, 2021).
78. J. Schwenk, S. Kim, J. Berwanger, F. Ghahari, D. Walkup, M.R. Slot, S.T. Le, W.G. Cullen, S.R. Blankenship, S. Vranjkovic, H.J. ug, Y. Kuk, F.J. Giessibl, J.A. Stroscio. Achieving μeV tunneling resolution in an *in-operando* scanning tunneling microscopy, atomic force microscopy, and magnetotransport system for quantum materials research. *Rev. Sci. Instrum.* **91**, 071101 (2020).
79. J. Hieulle, S. Luo, D.-Y. Son, A. Jamshaid, C. Stecker, Z. Liu, G. Na, D. Yang, R. Ohmann, L.K. Ono, L. Zhang, Y. Qi. Imaging of the atomic structure of all-inorganic halide perovskites. *J. Phys. Chem. Lett.* **11**, 818 (2020).
80. B. Ji, E. Rabani, A.L. Efros, R. Vaxenburg, O. Ashkenazi, D. Azulay, U. Banin, O. Millo. Dielectric confinement and excitonic effects in two-dimensional nanoplatelets. *ACS Nano* **14**, 8257 (2020).
81. J. Yamaguchi, H. Hayashi, H. Jippo, A. Shiotari, M. Ohtomo, M. Sakakura, N. Hieda, N. Aratani, M. Ohfuchi, Y. Sugimoto, H. Yamada, S. Sato. Small bandgap in atomically precise 17-atom-wide armchair-edged graphene nanoribbons. *Nature Commun. Mater.* **1**, 36 (2020).
82. S. Khatun, A. Banerjee, A.J. Pal. Nonlayered tellurene as an elemental 2D topological insulator: Experimental evidence from scanning tunneling spectroscopy. *Nanoscale* **11**, 3591 (2019).
83. B. Pécz, G. Nicotra, F. Giannazzo, R. Yakimova, A. Koos, A. Kakanakova-Georgieva. Indium nitride at the 2D limit. *Adv. Mater.* **33**, 2006660 (2021).
84. C. Murray, W. Jolie, J.A. Fischer, J. Hall, C. van Efferen, N. Ehlen, A. Grüneis, C. Busse, T. Michely. Comprehensive tunneling spectroscopy of quasifreestanding MoS_2 on graphene on Ir(111). *Phys. Rev. B* **99**, 115434 (2019).
85. A. Goriachko, P.V. Melnik, A. Schyrba, S.P. Kulyk, M.G. Nakhodkin. Initial stages of Bi/Ge(111) interface formation: A detailed STM study. *Surf. Sci.* **605**, 1771 (2011).
86. A. Goriachko, A. Schyrba, P.V. Melnik, M.G. Nakhodkin. Bismuth growth on Ge(111): Evolution of morphological changes from nanocrystals to films. *Ukr. J. Phys.* **59**, 805 (2014).
87. W. Melitz, J. Shena, A.C. Kummel, S. Lee. Kelvin probe force microscopy and its application. *Surf. Sci. Rep.* **66**, 1 (2011).
88. K. Müller, A. Goryachko, Y. Burkov, C. Schwiertz, M. Ratzke, J. Köble, J. Reif, D. Schmeißer. Scanning Kelvin probe and photoemission electron microscopy of organic source-drain structures. *Synth. Metal.* **146**, 377 (2004).

89. K. Müller, Y. Burkov, D. Mandal, K. Henkel, I. Paloumpa, A. Goryachko, D. Schmeißer. Microscopic and spectroscopic characterization of interfaces and dielectric layers for OFET devices. *Phys. Status Solidi A* **205**, 600 (2008).
90. D. Wrana, K. Cieślik, W. Belza, C. Rodenbücher, K. Szot, F. Krok. Kelvin probe force microscopy work function characterization of transition metal oxide crystals under ongoing reduction and oxidation. *Beilstein J. Nanotechnol.* **10**, 1596 (2019).
91. H.-C. Fu, V. Ramalingam, H. Kim, C.-H. Lin, X. Fang, H.N. Alshareef, J.-H. He. MXene-contacted silicon solar cells with 11.5% efficiency. *Adv. Energ. Mater.* **9**, 1900180 (2019).
92. W. Ki, X. Hei, H.T. Yi, W. Liu, S.J. Teat, M. Li, Y. Fang, V. Podzorov, E. Garfunkel, J. Li. Two-dimensional copper iodide-based inorganic–organic hybrid semiconductors: Synthesis, structures, and optical and transport properties. *Chem. Mater.* **33**, 5317 (2021).
93. J. Shakya, S. Kumar, D. Kanjilal, T. Mohanty. Work function modulation of molybdenum disulfde nanosheets by introducing systematic lattice strain. *Nature Sci. Rep.* **7**, 9576 (2017).
94. P.D. Swartzentruber, M.J. Detisch, T.J. Balka. Composition and work function relationship in Os–Ru–W ternary alloys. *J. Vac. Sci. Technol. A* **33**, 021405 (2015).
95. O.T. Hofmann; J.-C. Deinert; Y. Xu; P. Rinke; J. Stähler; M. Wolf; M. Scheffler. Large work function reduction by adsorption of a molecule with a negative electron affinity: Pyridine on ZnO(1010). *J. Chem. Phys.* **139**, 174701 (2013).
96. A. Asyuda, M. Gartner, X. Wan, I. Burkhart, T. Saßmannshausen, A. Terfort, M. Zharnikov. Self-assembled monolayers with embedded dipole moments for work function engineering of oxide substrates. *J. Phys. Chem. C* **124**, 8775 (2020).
97. Y. Zhou, C. Fuentes-Hernandez, J. Shim, J. Meyer, A.J. Giordano, H. Li, P. Winget, T. Papadopoulos, H. Cheun, J. Kim, M. Fenoll, A. Dindar, W. Haske, E. Najafabadi, T.M. Khan, H. Sojoudi, S. Barlow, S. Graham, J.-L. Brédas, S.R. Marder, A. Kahn, B. Kippelen. A universal method to produce low–work function electrodes for organic electronics. *Science* **336**, 327 (2012).
98. K.J. Rietwyk, D.A. Keller, A. Ginsburg, H.-N. Barad, M. Priel, K. Majhi, Z. Yan, S. Tirosh, A.Y. Anderson, L. Ley, A. Zaban. Universal work function of metal oxides exposed to air. *Adv. Mater. Interf.* **6**, 1802058 (2019).
99. G. Gaertner, D. den Engelsen, Hundred years anniversary of the oxide cathode – A historical review. *Appl. Surf. Sci.* **251**, 24 (2005).
100. H. Yuan, S. Chang, I. Bargatin, N.C. Wang, D.C. Riley, H. Wang, J.W. Schwede, J. Provine, E. Pop, Z.-X. Shen, P.A. Pianetta, N.A. Melosh, R.T. Howe. Engineering ultra-low work function of graphene. *Nano Lett.* **15**, 6475 (2015).
101. F. Jin, A. Miruko, D. Litt, K. Zhou. Functionalized carbon nanotubes for thermionic emission and cooling applications. *J. Vac. Sci. Technol. A* **40**, 013415 (2022).
102. M.C. James, M. Cattelan, N.A. Fox, R.F. Silva, R.M. Silva, P.W. May. Experimental studies of electron affinity and work function from aluminium on oxidised diamond (100) and (111) surfaces. *Phys. Status Solidi B* **258**, 2100027 (2021).
103. F. Fogarty, N.A. Fox, P.W. May. Experimental studies of electron affinity and work function from titanium on oxidised diamond (100) surfaces. *Funct. Diamond* **2**, 103 (2022).
104. S. Ullah, G. Wan, C. Kouzios, C. Woodgate, M. Cattelan, N. Fox. Structure and electronic properties of tin monoxide (SnO) and lithiated SnO terminated diamond (100) and its comparison with lithium oxide terminated diamond. *Appl. Surf. Sci.* **559**, 149962 (2021).
105. P. Schindler, D.C. Riley, I. Bargatin, K. Sahasrabuddhe, J.W. Schwede, S. Sun, P. Pianetta, Z.-X. Shen, R.T. Howe, N.A. Melosh. Surface photovoltage-induced ultralow work function material for thermionic energy converters. *ACS Energ. Lett.* **4**, 2436 (2019).
106. Y. Yu, D. Lee, B. Jeong. The dependence of the work function of Pt(111) on surface carbon investigated with near ambient pressure X-ray photoelectron spectroscopy. *Appl. Surf. Sci.* **607**, 155005 (2023).
107. T. Yamada, T. Masuzawa, H. Mimura, K. Okano. Electron emission from conduction band of heavily phosphorus doped diamond negative electron affinity surface. *J. Phys. D* **49**, 045102 (2016).
108. S. Ullah, N. Fox. Modification of the surface structure and electronic properties of diamond (100) with tin as a surface termination: A density functional theory study. *J. Phys. Chem. C* **125**, 25165 (2021).
109. M.T. Greiner, L. Chai, M.G. Helander, W.-M. Tang, Z.-H. Lu. Transition metal oxide work functions: The influence of cation oxidation state and oxygen vacancies. *Adv. Funct. Mater.* **22**, 4557 (2012).
110. K. Akada, S. Obata, K. Saiki. Work function lowering of graphite by sequential surface modifications: Nitrogen and hydrogen plasma treatment. *ACS Omega* **4**, 16531 (2019).
111. S. Naghdi, G. Sanchez-Arriaga, K.Y. Rhee. Tuning the work function of graphene toward application as anode and cathode. *J. Alloy. Compd.* **805**, 1117 (2019).

Received 14.08.23.
Translated from Ukrainian by O.I. Voitenko

М.В. Стріха, А.М. Горячко

ПОВЕРХНІ ЗІ ЗНИЖЕНОЮ РОБОТОЮ ВИХОДУ: ПРОБЛЕМИ СТВОРЕННЯ ТА ТЕОРЕТИЧНОГО ОПИСУ. ОГЛЯД

Дано огляд експериментальних робіт зі створення сучасних фотокатодів чи ефективних катодів для польової емісії зі зниженою роботою виходу або низькою/негативною електронною спорідненістю. Викладено теоретичні моделі для опису зниження електронної спорідненості під впливом заряджених шарів на поверхні напівпровідника/діелектрика.

Описано сучасні експериментальні методики визначення роботи виходу/електронної спорідненості та технології одержання поверхонь з низькими значеннями роботи виходу та електронної спорідненості. У рамках побудованої авторами простої теоретичної моделі показано, що наявність на поверхні напівпровідника дипольного шару (напр., з негативно заряджених атомів кисню й позитивно заряджених атомів рідкісноземельного металу) за умови рівності концентрацій різнойменно заряджених адсорбованих атомів може призвести до зниження спорідненості електрона на величину до 3 еВ. Також показано, що асиметрія поверхневих концентрацій кисню і металу може призвести до двох протилежних наслідків: при переважанні негативно зарядженого кисню зниження спорідненості робиться меншим через вигин зон угору в області просторового заряду напівпровідника, а при переважанні позитивно зарядженого металу зниження спорідненості стає більшим через вигин зон униз. Такий результат дозволяє запропонувати технологічні рішення для одержання поверхонь з мінімальною роботою виходу для приладів сучасної емісійної електроніки. У рамках побудованої простої теоретичної моделі оцінено значення роботи виходу у функціоналізованому гідроксильними групами максені. На той час коли в нефункціоналізованому матеріалі воно складає ∼4,5 еВ і практично не залежить від кількості площин Ti та C (у діапазоні від 1 до 9), після функціоналізації воно знижується приблизно до 1,6 еВ і так само практично не залежить від кількості атомних площин у максені. Описано пошуки експериментальних шляхів створення сучасних катодів з низьким значенням роботи виходу чи електронної спорідненості. Результатом обробки поверхні, здійсненої в рамках таких підходів, має бути встановлення в приповерхневій області зразка просторового розділення електричних зарядів у напрямку, перпендикулярному до площини поверхні. Такий стан може характеризуватися просторовим розподілом уздовж цього напрямку позитивних та негативних зарядів з локалізацією або в двох відмінних атомних площинах, або відповідно в одній атомній площині та протяжній області простору (останнє, зазвичай, у випадку напівпровідникової підкладинки). Технології одержання таких поверхонь можуть базуватися на різноманітних методах нанесення адсорбатів на поверхню метала або напівпровідника: фізично-парове осадження, хімічно-парове осадження, осадження з рідкої фази, дифузія з об'єму підкладинки, тощо. Окремо звернено увагу на ті експериментальні роботи, де на основі адсорбції рідкісноземельних металів (Ce, Gd, Eu) та коадсорбції кисню на поверхнях Si, Ge та Mo, в т.ч. в наноструктурованому стані, можуть утворюватися подвійні заряджені шари, що суттєво знижують роботу виходу.

Ключові слова: поверхня, робота виходу, електронна спорідненість, катод, дипольний шар.